Structural and dynamical roles of bound polymer chains in rubber reinforcement

Daniel Salatto[1], Jan-Michael Y. Carrillo[2], Maya K. Endoh[1], Takashi Taniguchi[3], Benjamin M. Yavitt[1], Tomomi Masui[4], Hiroyuki Kishimoto[4], Madhusudan Tyagi[5,6], Alexander E. Ribbe[7], Victoria Garcia Sakai[8], Margarita Kruteva[9], Bobby G. Sumpter[2], Bela Farago[10], Dieter Richter[9], Michihiro Nagao[5,6,11,*], Tadanori Koga[1,12,*]

[1]Department of Materials Science and Chemical Engineering, Stony Brook University, Stony Brook, New York 11794-2275

[2]Center for Nanophase Materials Sciences, Oak Ridge National Laboratory, Oak Ridge, Tennessee, 37831

[3]Graduate School of Engineering, Department of Chemical Engineering, Kyoto University, Katsura-Campus, Nishikyo-ku, Kyoto, 615-8510, Japan

[4]Sumitomo Rubber Industries Ltd., 1-1, 2-chome, Tsutsui-cho, Chuo-ku, Kobe, 671-0027, Japan

[5]NIST Center for Neutron Research, National Institute of Standards and Technology, Gaithersburg, Maryland, 20899-6102

[6]Department of Materials Science and Engineering, University of Maryland, College Park, Maryland 20742

[7]Department for Polymer Science & Engineering, University of Massachusetts, Amherst, MA 01003

[8]ISIS Pulsed Neutron and Muon Facility, Science and Technology Facilities Council
Rutherford Appleton Laboratory, Harwell Campus, Didcot OX11 0QX, United Kingdom

[9]Jülich Centre for Neutron Science (JCNS), Forschungszentrum Jülich GmbH, 52428 Jülich, Germany

[10]Institut Laue–Langevin, 6 rue Jules Horowitz, BP 156-38042, Grenoble Cedex 9, France

[11]Department of Physics and Astronomy, University of Delaware, Newark, Delaware, 19716

[12]Department of Chemistry, Stony Brook University, Stony Brook, New York 11794-3400

***Corresponding Authors**

tadanori.koga@stonybrook.edu (T. K.)

michihiro.nagao@nist.gov (M. N.)

For Table of Content use only

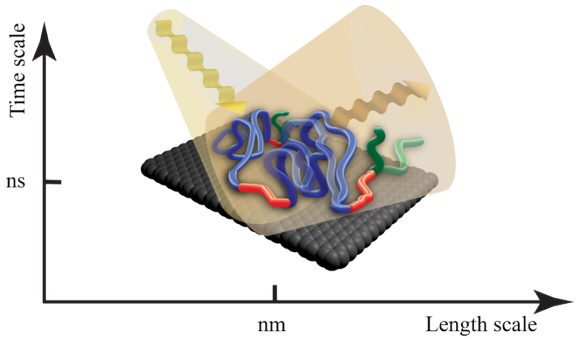

Abstract

The addition of nanofillers to rubber matrices is a powerful route to improve the mechanical properties. Here we focus on a molecular understanding of basic mechanisms that are important for the reinforcement in rubbers. The key role in this process is ascribed to bound rubber (BR) that engages with the matrix as well as with adjacent nanofillers. So far, this understanding is impeded by the lack of experimental tools to directly probe the BR chains buried in a polymer matrix composed of the same polymer. To tackle this challenge, we combine neutron scattering/spectroscopy techniques with isotope-labeling and molecular dynamics simulations. The system is a simplified carbon black-filled polybutadiene. The combined experimental and computational results provide new insight into the local structural and dynamical heterogeneities of the BR chains and their interactions with the matrix polymer, highlighting (i) the structural partition of the bound chains into three components (*i.e.*, trains, loops, and tails) with their fractions; (ii) their dynamical hierarchies, *i.e.*, the trains that remain immobile on the filler surface, the loops that are fairly large and hence allow the interdigitation of matrix chains, and the tails with their unique characteristics to reach far out into the matrix and entangle with matrix chains. These multiple roles of the constituent components of the BR chains promote the formation of a well-developed adhesive polymer-filler interface, enhancing the elastic property of a filled rubber. The comprehensive understanding derived and validated with the model rubber will be translatable to many other polymer nanocomposites.

I. Introduction

Polymer nanocomposites (PNC) continue to be of significant fundamental scientific and applied interest given their rich array of structural, dynamical and mechanical behaviors that involve both polymer and colloid science aspects.[1, 2] Carbon black (CB) filled rubbers are known as the most successful polymer nanocomposites (PNCs) in industry.[3] The typical sizes of primary CB fillers used for automobile tires range from a few tens of nanometers to 100 nm. Hence, compared to micrometer-sized fillers, the surface area of nanofillers increases significantly, magnifying the importance of polymer-filler interfaces.[4] In addition, CB fillers used for automobile tires are not chemically modified, in contrast to "polymer grafted nanoparticles" on which many experiments and simulations in polymer melts have been reported.[2, 5]

Twiss made the first observation in 1925 on the effect of "bound rubber (BR)"[6] (*i.e.*, polymer chains that *physically* adsorb on the surfaces of CB fillers and are resistant to dissolution in a good solvent) on improved mechanical properties of rubbers. In addition, the existence of an interphase with the properties between those of the BR and the bulk has been indicated.[7-12] There is general agreement that the BR[13-18] and/or interphase are critical parameters for rubber reinforcement. It should be noted that the BR layer corresponds to the "bound polymer layer" observed in other PNCs whose thickness is commensurate with the radius of gyration (R_g) of adsorbed polymer chains.[19-27] At high filler loadings (such as those required for commercial tire products) where the interparticle distance between neighboring fillers is of the order of the thickness of the BR chains, the BR chains begin to interfere and overlap with each other.[4, 22, 28] This in turn results in the formation of a filler network structure via the BR chains as polymer "bridges" between neighboring fillers.[28-32] Among several factors contributing to mechanical property enhancement, this filler-filler network formed via polymer bridges is considered as the most significant.[33, 34] However, a molecular understanding of basic mechanisms that are important for the reinforcement in rubber, a topic of utmost importance for the molecular design of tires, is still being debated in this comparatively mature field.[1] The main reason for this problem is the lack of experimental tools to directly probe the bound chains and/or interphase buried in a polymer matrix composed of

the same polymer. Instead, many simulation studies have shed light on the structures and dynamics of polymer chains at the polymer/filler interface.[2, 5, 35] For instance, Starr and co-workers[36] demonstrated that the polymer chains are elongated and flattened near the filler surface regardless of the polymer-filler interactions, while a gradient of segmental relation occurs when the polymer-filler interaction is attractive.[36, 37]

The inner structure of an irreversibly adsorbed polymer layer on a solid surface is very different from that of a chemically grafted polymer layer because each adsorbed chain has many contact points with a solid surface.[38-40] These theories proposed that the adsorbed chains are made up of different types of segment sequences, *i.e.*, "trains" (adsorbed segments), "loops" (sequences of free segments connecting successive trains), and "tails" (non-adsorbed chain ends). The train/loop/tail picture of physisorbed polymer chains has been qualitatively confirmed for a planar solid surface using neutron reflectivity.[41] As will be discussed later, the CB filler used in this study can be approximated as a "planar" geometry such that the same train/loop/tail picture can be adopted for the BR formed on the CB filler, giving rise to a hierarchy of the structures and dynamics at the segment and chain levels. This resultant local heterogeneity thereby creates additional complications for understanding the molecular mechanisms behind the enhancement of macroscopic properties of PNCs.

In this article, we investigate the in-situ structures and dynamics of BR chains in a chemically identical polymer matrix. The techniques used are small-angle neutron scattering (SANS), neutron backscattering (NBS), and neutron spin echo (NSE). A spherical CB filler filled in monodisperse polybutadiene (PB) is chosen as a model. A BR layer on the surface of CB fillers is prepared by using hydrogenated or protiated polybutadiene (hPB), while the matrix is composed of deuterated polybutadiene (dPB). The scattering length density (*i.e.*, the neutron contrast) of CB is nearly identical to that of dPB, allowing us to selectively label the BR layer and creating strong contrast between the matrix and BR.[21] We previously reported the contrast-matched SANS/NSE studies on the in-situ structures and dynamics of the BR (composed of a similar molecular weight of hPB on the same CB surfaces) dispersed in a good solvent[21] as well as in polymer solutions.[25] The results

demonstrated that the BR is composed of two regions regardless of polymer concentrations ($c_p \leq 1.83\ c^*$, where c^* is the overlap polymer concentration[42]) in solutions: an inner unswollen region of about 0.5 nm-thick and an outer swollen region where the polymer chains display a parabolic profile with a diffuse tail. In addition, the NSE results showed that the collective dynamics of the swollen BR chains in a good solvent and in dilute polymer solutions can be explained by the so-called "breathing mode".[43] We further discussed the formation mechanism of the interphase between the BR and free polymer chains in polymer solutions.[25] The present study continues these investigations but on a more realistic system that mimics the automobile tire, by replacing the matrix with a chemically identical polymer melt. The volume concentration of CB filler is set to 20%, which is below the percolation threshold (≈ 30 % (**Figure S1A&B**)). In addition, coarse-grained molecular dynamics (MD) simulations are performed to complement the experimental results and unravel details that are not accessible experimentally.

We present the following results about the interfacial structures and dynamics of the BR in the melt: (i) the BR layer is composed of the inner layer, which consists of the train segments and does not allow any penetration of matrix polymer chains, and the outer layer, which is composed of loops with a broad size distribution and tails that extends well into the matrix. The BR layer is also stable against temperatures that are far above the bulk glass transition temperature (T_g); (ii) the trains are immobile within the NBS/NSE time widow (t < 500 ns), while the loops have a mobility gradient as a function of the distance from a filler surface and the tails, which reach far out into the matrix, move in the same manner as free chains in the melt; (iii) the average local dynamics of the loops and tails observed by NBS remain unchanged between the bound chains and free chains; (iv) the "confinement length" of the BR chains observed by

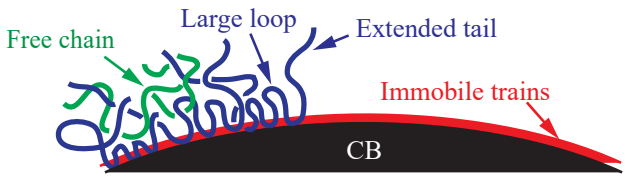

Figure 1. Schematic view of the BR chains highlighting the novel characteristics of the three segment sequences revealed by the present study is shown. The immobile train components promote the strong foundation of the BR chains on the filler surface and the large loops and tails play vital roles to build a strong interlocking interphase between the BR and polymer matrix.

NSE, which limits the monomer motions by the size, shows a much weaker temperature dependence compared to the bulk due to the contribution of the loops fixed at their anchor points; (v) the BR chains entangle (for the tails) or interdigitate (for the loops) with the free chains in the matrix. Hence, as summarized in **Figure 1**, the present results reveal that the trains are immobile within the experimental timescales and act as strong anchoring points. At the same time, the chain entanglement/interdigitation leads to a well-developed adhesive interphase between the filler and matrix polymer. The interactions with the matrix polymer cause additional interfacial frictions, reducing the flow of the matrix polymer and thus enhancing the elastic property, as demonstrated in **Figure S2**.

II. Experimental Section

II.1. Materials. We simplified the material system by using a spherical CB filler (Asahi Carbon Co., Japan) with mostly non-fused aggregates and monodisperse PB. As previously reported[44], CB fillers are typically fused together, resulting in the smallest unbreakable unit of CB fillers. The unbreakable unit is further clustered into higher order structures in a rubber matrix. The unbreakable unit and the higher-order structure are called as an aggregate and agglomerate, respectively, in the context of the common terminology in this field.[45] We here adopt the same terminologies to identify the hierarchical structures of the CB filler in the PB matrix. Based on transmission electron microscopy (TEM) experiments, the mean radius of the primary CB fillers was previously determined to be R_{TEM} = (43 ± 20) nm[21]. The error bars used in this paper represent ±1 standard deviation unless otherwise noted. In addition, small-angle x-ray scattering experiments for the bare CB fillers (without BR) dispersed in toluene after application of a sonic field gave the radius of gyration ($R_{g,CB}$) to be (49 ± 5) nm[21], which is slightly larger than that of the primary CB particles assuming a spherical shape ($R_{g,TEM} = \sqrt{3/5}\, R_{TEM} = 33$ nm). Hence, on the basis of the volume consideration, it may be reasonable to deduce that about 3 ($=(R_{g,CB} / R_{g,TEM})^3$) CB primary particles are fused together into the unbreakable unit (or aggregates). Therefore, the effect of

occluded rubber trapped between fused CB fillers[34] on reinforcement can be minimized. The presence of the CB aggregates in the dPB matrix was further confirmed by TEM experiments and the average size of the CB aggregates is in good agreement with the aforementioned SAXS result (**Figure S1C and E**). On the other hand, the morphological characterization of the agglomerate using TEM is not practical because the size is expected to be comparable or greater than the thickness of an ultrathin film (approximately 100 nm) used for TEM experiments. Instead, we utilized ultra-small-angle X-ray scattering (USAXS) to estimate the size of the CB agglomerate in the rubber.

The CB fillers were first dissolved in toluene and then added to the PB solutions, which are subsequently sonicated for 1 hour. The solvent was then evaporated from the mixed solution, and the composite samples were annealed at 100 °C for 3 hours. The BR was composed of hPB (weight average molecular weight (M_w) = 45,100 g/mol, polydispersity index ($Đ$) = 1.08, 1,4 addition = 80 %, Sumitomo Rubber). The BR-coated CB fillers were then extracted by a solvent leaching process (the details have been described elsewhere[21]). In brief, the resultant CB/PB compounds were dissolved in toluene and dispersed using an ultrasonic bath for about (1 to 3) hours. Afterwards, the solution was left for some time to let the incomplete BR-coated CB fillers precipitate. The top homogenous portion of the solution, where the BR-coated CB fillers were present, were collected and further separated through centrifugation. We repeated the series of operations for several times to purify the final BR-coated CB fillers. The resultant "BR-coated CB fillers" solution was then mixed in a fully deuterated PB (dPB, M_w = 50,200 g/mol, $Đ$ = 1.08, 1,4 addition = 80 %, Polymer Sources Inc.,)/toluene solution. The filler loading (ϕ) was set to a volume fraction of 20 %. The solvent was then evaporated from the mixed solution and the composite samples were further dried in a vacuum oven at 100 °C for a prolong period of time (~ 7 days). The thickness of the BR in the dry state (without a polymer matrix) was estimated to be (4.5 ± 0.5) nm by using TEM experiments.[21] Hereafter we assign the sample as "BR-coated CB in dPB". We also prepared the CB filler (without a protiated BR layer) embedded in dPB with ϕ = 0.2 (hereafter assigned as "CB in dPB") as control.

II-2. Techniques

TEM experiments

Samples for TEM were prepared via cryo-ultramicrotomy at -120 °C using a diamond knife. Sections were collected using ultrathin carbon (~ 3 nm) coated grids and allowed to warm to room temperature before transfer to a JEOL 2200FS EFTEM operated at 200 kV. The unstained samples were cooled to -180 °C in the TEM and imaged using zero-loss filtered mode with an energy width of 20 eV.

USAXS experiments

USAXS measurements were performed at the BL20XU, SPring-8 (Hyogo, Japan) to characterize the BR-coated CB fillers in the dPB matrix, while the BR (composed of hPB) in the dPB matrix is not visible due to the lack of an X-ray contrast. The X-ray energy was 23 keV and the sample to detector distance is 160.5 m. A pixel-array detector (PILATUS 100K, Dectris ltd.) was used to obtain the USAXS data.

SANS Experiments

SANS experiments were performed at the NCNR. The BR-coated CB in dPB sample was filled in custom-made titanium cells with quartz windows available for the SANS experiments. The details of the SANS experiments including the correction of incoherent scattering[46] have been described elsewhere.[21, 25] SANS measurements were taken at 4 different sample-to-detector distances, 1 m, 4 m, 13 m, and 15.5 m using the NG7-30m and NGB-30m SANS instruments. The wavelengths (λ) of the incident beams were 0.6 nm and 0.81 nm. The scattered intensity was azimuthally averaged and corrected for the background of the cell, the electronic noise and sensitivity of the detector, to calibrate in the absolute unit and then stitched together to an observed q range of 0.015 nm^{-1} to 4.6 nm^{-1}. The incoherent scattering was estimated to be 0.032 cm^{-1} for the BR-coated CB in dPB sample.[25] The temperature for the samples was varied from 25 °C to 150 °C with the temperature accuracy better than 1 °C.

As previously reported, we have established a SANS technique to identify the scattering from the BR on the same CB, which originates from the density heterogeneity in the BR layer, dispersed in a good solvent[21] and polymer solutions.[25] We here applied the similar strategies to the BR-coated CB in dPB sample. Since the CB primary particles have relatively large polydispersity, the distinct scattering maxima from a monodisperse core (i.e., the CB aggregate)-shell (i.e., the BR) type form factor do not appear.[21, 25] We first evaluated the hierarchical structures of the core (CB) alone in the dPB sample (i.e., the CB in dPB sample). The scattering from the hierarchical structures of the BR-coated CB fillers in the dPB matrix was then calculated by using the unified (UF) equation[47] with the individual structural parameters of the core and the shell determined above. Lastly, we subtracted the calculated scattering intensity using the UF equation from the observed SANS profile for the BR-coated CB in dPB sample, resulting in the excess scattering from the inner structure of the BR.

NSE Experiments

By using NSE, we observed coherent scattering from protiated polymer chains in the deuterated polymer melt at the length (2 nm to 10 nm) and time scales (0.02 ns to 500 ns). NSE measurements were carried out on the CHRNS-NSE instrument at the NCNR and the IN15 at the ILL. The wavelength of the incident beam was 0.6 nm and 1.1 nm at the NCNR and 1.0 nm and 1.35 nm at the ILL. Measurements were taken at the four q values at 0.8 nm^{-1}, 1.1 nm^{-1}, 1.5 nm^{-1}, and 2.0 nm^{-1}. The Fourier time range was covered up to 100 ns at the NCNR, while it was further extended to 500 ns at the ILL. The NSE data taken on the CHRNS-NSE was reduced by using the Data Analysis and Visualization Environment (DAVE) software,[48] while IN15 data was treated by the Igor macro developed for the instrument and normalized intermediate, scattering functions were calculated for each sample. The experiments were carried out under vacuum to prevent possible polymer degradation. The original IN15 data are curated under the reference: https://doi.ill.fr/10.5291/ILL-DATA.9-12-560.

NBS Experiments

NBS measurements, which provide the spatial (sub nm to 1 nm) and temporal (0.1 ns to 2 ns) information, were carried out at the High Flux Backscattering Spectrometer (HFBS) at the NCNR.[49] The instrument was used to capture full quasi-elastic spectra as a function of energy transfers. As the incoherent scattering cross section of hydrogen dominates neutron scattering in the measured q-range, the quasi-elastic scattering originates mostly from the self-motion of H atoms through energy change of the scattered neutrons. It should also be noted that deuterium scatters incoherently, while the contributions are much smaller than H atoms. As will be discussed later, we considered these contributions for the data analysis. At the same time, Richter and co-workers showed that 1,4 PB shows a static structure peak at $q \approx 15$ nm^{-1} and the characteristic time of the collective dynamics was about 1 ps at room temperature.[50] Since this time window is completely outside the dynamic range of the instrument, the contributions from the collective dynamics of the dPB matrix are ignored. For quasi-elastic spectra, measurements were made between 10 h and 12 h in order to acquire good statistics and Doppler was operated to achieve ± 17 μeV dynamic range. The measured energy range was up to $E = 17$ μeV with 0.85 μeV resolution. Sample temperature was equilibrated for 30 mins before measurements. Data was collected in the standard q range of 2.5 nm^{-1} to 17.5 nm^{-1}. The instrument resolution was measured by measuring sample at T = 4K where sample is expected to scatter elastically. The DAVE software[48] was utilized to conduct the analysis.

It should be noted that the same BR-coated CB in dPB and hPB in dPB samples were used for NSE experiments at the CHRNS-NSE first, then for NBS experiments, and finally for NSE experiments at the ILL. As shown in **Figure S3**, the $S(q,t)/S(q,0)$ for the BR-coated CB in dPB measured at CHRNS-NSE and ILL show an excellent agreement each other except for long times (due to the resolution limit for the CHRNS-NSE instrument), ruling out the possibility of sample degradation.

MD Simulations

We performed coarse-grained MD simulations to study the structures and dynamics of polymer chains that are adsorbed on a highly adsorbing surface (representing CB) in a polymer matrix based on the established protocol.[51]. Since the size of CB fillers by far exceeds the BR thickness, the simulation box was treated as a slab configuration[25] where it has periodic boundary conditions in both *x* and *y* axes, but not in the *z* axis. An attractive substrate, made up of Lennard-Jones beads arranged in a hexagonal closed pack lattice, was placed such that it serves as a boundary at $z = 0$. Fully flexible polymer chains with degree-of-polymerization, N_{MD} = 2,000, which is well above the critical entanglement length (N_e = 30 for 1,4 PB[52]) and is in a similar order of magnitude compared to that of the experimental one (N_{ex}=833)), were utilized.

The interaction between all beads is described by the truncated-shifted Lennard-Jones (LJ) potential,

$$U_{LJ}(r) = \begin{cases} 4\varepsilon_{LJ}\left[\left(\frac{\sigma}{r_{ij}}\right)^{12} - \left(\frac{\sigma}{r_{ij}}\right)^{6} - \left(\frac{\sigma}{r_{cut}}\right)^{12} + \left(\frac{\sigma}{r_{cut}}\right)^{6}\right] & r < r_{cut} \\ 0 & r \geq r_{cut} \end{cases} \quad (1)$$

where r_{ij}, is the distance between the i^{th} and j^{th} bead, ε_{LJ} is the well depth. r_{cut} is the cutoff, which is equal to 2.5σ (where σ is the diameter of a Lennard-Jones bead) for monomer to substrate interactions (*i.e.*, a short-ranged attractive substrate) and $2^{1/6}\sigma$ for the monomer-to-monomer interactions (*i.e.*, purely repulsive monomers). The interaction parameter (ε_{LJ}) between monomer beads and substrate beads was set to 8 k_BT (k_BT is the thermal energy). Experimentally, it is not straightforward to quantify this value since the surface tension of a CB filler varies, depending on a number of factors including surface activity, chemical functionality, microstructure, and preparation.[14, 53] In addition, multiple attachment sites of bound chains to filler surfaces render the estimation of surface activity more difficult.[54] Richter and co-workers[55] previously performed density functional theory calculations to estimate the polymer/surface interaction energy between various polymers and a silica (SiO_2) surface. The results showed that the interaction energy of PB

with Si-OH, which is weaker than that between CB and PB,[56] was about $5k_BT$. Furthermore, as discussed below, the MD results with the given ε_{LJ} represent the experimental results in a satisfactory manner. Hence, we believe that the interaction parameter used is reasonable to mimic the experimental conditions. The connectivity of monomers into polymer chains was maintained by the finite extension nonlinear elastic (FENE) potential,[57]

$$U_{FENE}(r) = -\frac{1}{2}k_s R_m^2 \ln\left(1 - \frac{r^2}{R_m^2}\right) \quad (2)$$

with the spring constant $k_s = 30.0\ k_BT/\sigma^2$, and maximum bond length $R_m = 1.5\ \sigma$.

At the chain level, we defined a polymer bead as being adsorbed on to the substrate if its distance to a surface bead is less than 1.18 σ[25] which is a little over $2^{1/6}\ \sigma$ – or the minimum of the LJ 6–12 potential describing the interaction between polymer chain and substrate beads. A train is a series of adsorbed connected beads; a tail is a series of connected beads with one end being adsorbed and the rest of the beads are unadsorbed and the ends is one of the chain ends; a loop is a series of connected beads where the end beads are adsorbed beads.

To minimize finite size effects, the x and y dimensions were set to a much larger value (*i.e.*, $\approx$ 120 σ) than the bulk value of the square root of the mean square end-to-end distance of the polymer ($\approx$ 60 σ). To mimic the experimental situations, we first created bound chains on a solid surface by the simulation protocol previously established.[25] The production run of the MD simulations involves running the system in an canonical (NVT) ensemble using a Langevin thermostat with an integration timestep 0.01 τ and proceeded to up to 10^6 τ, where $\tau \equiv \sigma (m/k_BT)^{1/2}$ (m is the mass of a bead) is the characteristic time. The details of the MD simulations including the box sizes and the numbers of free and bound polymer chains are tabulated in **Table 1**.

Table 1. Simulation details used for this study.

Degree of polymerization	2,000
Box Size (L_x, L_y, L_z)	120 × 120 × 398 σ^3
Total number of beads	4,913,920
Number of free chains	2,400
Number of bound chains	41
Average number of tails per bound chain	1.4
Average number of trains per bound chain	48.5
Average number of loops per bound chain	47.5
Average degree of polymerization for tails	501.4
Average degree of polymerization for trains	8.4
Average degree of polymerization for loops	18.9

III. Results and Discussion

III. 1. Structures of Bound Rubber - Small Angle Scattering

We briefly discuss the SANS result for the CB in dPB sample. The detailed analysis is summarized in the SI. As shown in **Figure S4A**, the SANS data for the CB in dPB sample showed the power-law scattering (i.e., $I(q) \sim q^{-p}$) at 0.09 nm^{-1} < q < 0.3 nm^{-1} with p = 3.10 $\pm$ 0.05. This indicates that the surface of the primary CB fillers is "rough" described by a surface fractal[44, 58]. Moreover, there is additional scattering originated from an internal inhomogeneous (the so-called turbostratic) structure (i.e., voids) within the CB fillers whose size is less than 1 nm[59]. We estimated the contribution[44] (see **Figure S4B**) and subtracted it from the observed scattering for the BR-coated CB filler in dPB.

Figure 2A shows the SANS result for the BR-coated CB filler in dPB at 150 ℃, q is the magnitude of the scattering vector defined by $q = (4\pi/\lambda)\sin(\theta/2)$, where θ is the scattering angle and λ is the wavelength of an incident neutron beam, respectively. At the same time, USAXS, which allows us to extend the low q-value to 3.5 × 10^{-3} nm^{-1} (**Figure 2A** indicated in blue), was

utilized to characterize the hierarchical structures of the BR-coated CB fillers in the dPB matrix. Note that USAXS is not sensitive to the BR (composed of hPB) in the dPB matrix due to the lack of an X-ray contrast between hPB and dPB. Using the Guinier scattering function (i.e., the first term in the right-hand side of eq. (3)), we estimated the radius of gyration of BR-coated CB agglomerates (without the BR thickness). The best-fit to the data (represented by the black line in the inset) gave us the radius of gyration of BR-coated CB agglomerates to be 125 $\pm$ 5 nm (without the BR thickness). We also confirmed that the agglomerates do not form percolated structures in the matrix at ϕ= 0.2 by independent mechanical experiments and electric conductive experiments (**Figure S1A and B**).

Given the USAXS data, we applied the unified (UF) equation[47] to the SANS data (**Figure 2A**) and characterized the hierarchical structures of the BR-coated CB fillers in the polymer matrix. In this case, the UF equation is given by eq. (3)[60]:

$$I(q) = A\exp\left(-\frac{q^2R_{g,1}^2}{3}\right) + B\left[\mathrm{erf}\left(\frac{qR_{g,1}}{\sqrt{6}}\right)^3/q\right]^{\nu} \times \exp\left(-R_{g,2}{}^2q^2/3\right) + C\exp\left(-\frac{q^2R_{g,2}^2}{3}\right) + D\left[\mathrm{erf}\left(\frac{qR_{g,2}}{\sqrt{6}}\right)^3/q\right]^{\beta} \quad (3)$$

where $R_{g,1}$ is the radius of gyration of the BR-coated CB agglomerates which is approximated as the sum of the size of the CB agglomerates (obtained from the aforementioned USAXS results) and the shell (BR) thickness, giving us $R_{g,1}$=129.5 nm. The radius of gyration of the primary BR-coated CB aggregates, $R_{g,2}$ was estimated previously to be 53.5 nm (*i.e.*, the R_g of the core of 49 nm plus the thickness of the shell (i.e., 4.5 nm) that was estimated by TEM after solvent leaching).[21] The power-law exponents of ν and β are related to the surface structures of the BR-coated CB aggregates and their agglomerates. *A*, *B, C,* and *D* are numerical constants.[47] According to a previous study,[60] the surface fractal of bound rubber formed on a filler surface is expected to be identical to that of a filler surface, and we therefore set the ν and β values to 3.1. The best-fit of eq. (3) with the parameters of $R_{g,1}$ = 129.5 nm, $R_{g,2}$ = 53.5 nm, and $\nu = \beta$ =3.1 to the SANS data is represented by the dotted line in **Figure 2A**. Hence, a deviation from eq. (3) at q > 0.1 nm^{-1} is

evidenced, indicating the presence of excess scattering originating from the inhomogeneity within the BR layer.

Representative excess scattering from the BR layer (**Figure 2B)** was calculated by subtracting the contributions of the hierarchical structures of the BR-coated CB fillers in the dPB (using eq. (3)) and the void structure of CB. The excess scattering originates from the local density heterogeneity due to the penetration of matrix chains to the BR layer (*i.e.*, polymer chain scattering). To analyze the excess scattering, the following three assumptions were made: (i) the CB filler is approximated as a "planar" geometry (see, the inset of **Figure 2C**) since the average diameter of CB far exceeds the BR thickness[21]; (ii) the BR is modeled as two layers, an inner layer composed of strongly adsorbed chains and an outer layer composed of loosely adsorbed chains, based on previous experimental[61, 62] and computational[63-65] results; (iii) the tails and loops of a BR chain can be approximated by a parabolic function according to a previous Monte Carlo study.[66] Hence, the following two-layer structural model was utilized to express the chain scattering from the hPB bound chains that are mixed with the dPB chains:

$$\varphi_0(z;z_1,\varphi_a,\varphi_m,L) = \begin{cases} \varphi_a & 0 \le z \le z_1 \\ \varphi_m\left[1-\left(\frac{z}{L}\right)^2\right] & z_1 \le z \le L \\ 0 & L \le z \end{cases} \quad (4)$$

where φ_a is the polymer volume fraction of the inner layer, φ_m is the extrapolated volume fraction to $z = 0$ from the outer layer (z is the distance from the solid surface), L is the cut-off thickness of the outer layer. Note that we fixed the φ_a value to be 1.0 based on the previous results for similar BR-coated CB fillers in a good solvent[21] or polymer solutions.[25] In addition, motivated by previous MD results where the formation of a well-developed interface between a polymer brush and a melt of identical chains was indicated,[9] we considered interfacial broadening to the density profile by convoluting eq. (4) with a normalized Gaussian function with an interfacial roughness of σ_s, as previously reported.[67] It should be emphasized that the data fitting was completely independent of the outcomes of the MD simulations to be discussed below.

The structure factor, $S(q)$, from the BR layer is then calculated by Fourier transform of φ

$\left(z;\{z_1,\varphi_a,\varphi_m,\sigma_s,\bar{L}\right)$, *i.e.*,

$$S(q) = c_{CB}V_p\rho_0^2\left|\frac{1}{l_{BR}}\int_0^\infty \varphi\left(z;\{z_1,\varphi_a,\varphi_m,\sigma_s,\bar{L}\right)\exp(iqz)\,dz\right|^2 \quad (5)$$

where ρ_0 is a scattering length density (*SLD*) difference between the BR (hPB, $SLD_{\mathrm{hPB}} = 0.4 \times 10^{10}$ (cm^{-2})) and matrix (dPB, $SLD_{\mathrm{dPB}} = 6.5 \times 10^{10}$ (cm^{-2})) and c_{CB} is the volume fraction of the BR. V_{p} is the volume of the bound layer, which can be approximated by $4\pi R_{CB}^2 l_{BR}$, where $R_{CB}$is the average radius of the CB filler and l_{BR} is the original thickness of the BR. $\bar{L}$ is the mean thickness of the BR layer in the dPB matrix. $\varphi\left(z;z_1,\varphi_a,\varphi_m,\sigma_s,\bar{L}\right)$ in the right-hand side is convoluted with a normalized Gaussian function $g\left(L;\bar{L},\sigma_s\right)$ with an interfacial roughness of σ_{s} and $\bar{L}$ as

$$\varphi\left(z;z_1,\varphi_a,\varphi_m,\sigma_s,\bar{L}\right) = \int_{-\infty}^{+\infty}\varphi_0(z;z_1,\varphi_a,\varphi_m,L\})g(L;\{\bar{L},\sigma_s\})dL \quad (6)$$

$$g\left(L;\bar{L},\sigma_s\right) \equiv \frac{1}{\sqrt{2\pi\sigma_s{}^2}}\exp\left(-\frac{1}{2\sigma_s{}^2}\left(L-\bar{L}\right)^2\right) \quad (7)$$

In addition, to ensure conservation of mass, the volume fraction profiles were integrated such that the amount of the polymer chains remained the same as the original thickness. The method of nonlinear least squares fitting was used. The sum of the squares of deviations (*SSD*) between the experimental ($S_{exp,i}$) and computed ($S_{com,i}$) values was calculated by $SSD = \sum_{i=0}^{n}(S_{exp,i} - S_{com,i})^2$.

Figure 2C shows the concentration profile obtained from the best-fit (the solid line in **Figure 2B**) to the data. **Figure S4C** verifies that the implementation of the inner layer with $\varphi(z) = \varphi_a$ is essential to fit the overall SANS data. The results indicate that the inner layer of z_1=0.43 $\pm$ 0.03 nm in thickness does not allow any penetration of matrix chains. This thickness is consistent with the previous study in a good solvent[21] and in polymer solutions.[25] In addition, the thickness, which is commensurate with the segment length (l) of a PB monomer ($l = l_o\sqrt{C_\infty * n_b} = 0.67\ nm$; where n_b is the average number of main chain bonds ($n_b = 3.86$), l_o is the length of one bond ($l_o = 0.15\ nm$), and C_∞ is the characteristic ratio ($C_\infty = 5.2$)) for PB,[52] suggests that

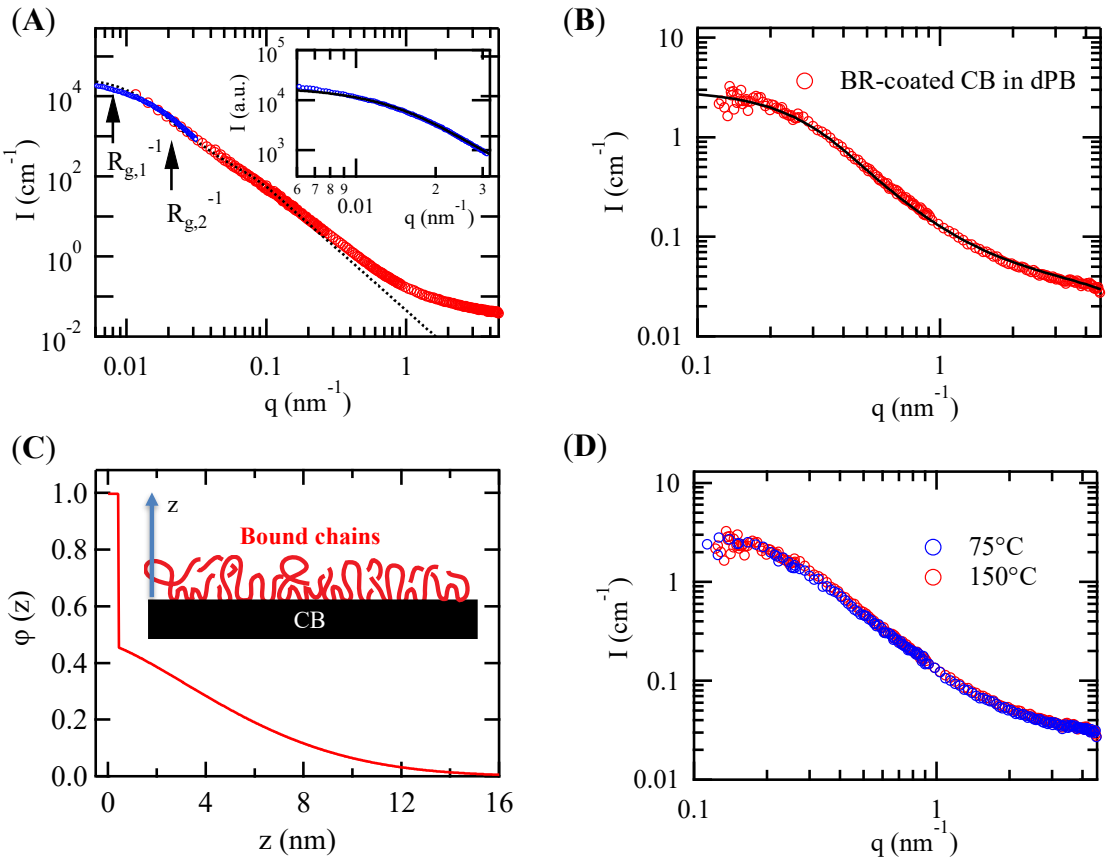

Figure 2. (**A**) SANS (indicated by red circles) and USAXS (indicated by blue circles) profiles for the BR-coated CB filler at 150 °C. The USAXS data was shifted vertically to overlap with the SANS data. Based on the USAXS data, we independently determined the radius of gyration of BR-coated CB aggregates (without the BR thickness) using eq. (3) but without the third and fourth terms in the right-hand side of eq. (3). The best-fit to the data (represented by the solid line in the inset) gave us the radius of gyration of BR-coated CB agglomerates to be 125 $\pm$ 5 nm (without the BR thickness). The dotted line in (A) corresponds to the best-fit of eq. (3) to the data. The two arrows marked by $R_{g,1}^{-1}$ and $R_{g,2}^{-1}$ indicates the existence of Guinier scattering with the radii of gyration $R_{g,1}$ and $R_{g,2}$. The fitting parameters were determined to be A=30,700 $\pm$ 135, B=0.0135 $\pm$ 0.0005, C=983 $\pm$ 35, and D=0.045 $\pm$ 0.008. (**B**) Excess scattering from the BR at 150 °C after the corrections described in the text. The best-fit of eq. (5) to the data is represented by the solid line. The $SSD/(n-p)$ value (where n is the total number of experimental data point and p is the number of derived variables in determining the model function) was 4.3 $\times 10^{-5}$. (**C**) Polymer concentration profile of the BR layer as a function of the distance from the filler surface (z) obtained from the SANS results. In the inset, the schematic view of the BR chains on the CB surface is shown. $\bar{L}$ = (8.4 $\pm$ 0.6) nm, φ_m = (0.46 $\pm$ 0.04), σ_s = (4.9 $\pm$ 0.5) nm, and z_1= (0.43 $\pm$ 0.03) nm were obtained from the best-fit. (**D**) Excess scattering from the BR at 75 °C and 150 °C are plotted. We confirmed that the overall shape of the excess scattering remains the same regardless of temperatures (up to 150 °C).

this inner region consists of the train segments of BR chains. This is further confirmed by the MD results, as will be discussed later. Moreover, it was found that the outer layer, which is composed of loops and tails, extends well into the matrix ($\bar{L}$ = 8.4 $\pm$ 0.6 nm and σ_s = 4.9 $\pm$ 0.5 nm), indicating that the tails are pushed outward by the dense layer of loops.[66] The total thickness of the BR (*i.e.*, $\approx$ 8.8 nm (or 0.43 nm + 8.4 nm)) is about 1 R_g (R_g of hPB is 7.9 nm, **Figure S4D**), which is in good agreement with previous reports.[23, 27] Furthermore, the overall structure of the BR layer remained unchanged at temperatures between room temperature and 150 °C (**Figure 2D**), which are far above the bulk T_g (~ - 90 °C), while the dynamics on the segment and chain levels are sensitive to temperature, as will be discussed later.

At the same time, the broadened density profile of the outer layer (**Figure 2c**) suggests the existence of different lengths of loops and tails. This supports the Guiselin's concept that physically adsorbed polymer chains with multiple solid-segment contacts are considered as a "polydisperse pseudo-brush"[40]. Guiselin also predicted that the polymer fraction of physically adsorbed chains in the melt decays by power-law, z^{-g} (g is a constant)[40]. Inspired by Guiselin's calculations, we also fit the excess scattering data with the polydisperse pseudo-brush model. The detailed analysis using the method of nonlinear least squares fitting is summarized in the SI. As shown in **Figure S5**, we found that the parabolic shape is more reasonable than a power-law profile to express the overall density profile of the BR in the melt. As will be discussed later, this is in line with the MD simulation results (**Figure 3A**). We shall further discuss the distributions of train/loop/tail components on the basis of the MD simulations. On the other hand, this broad outer layer also raises a concern of whether the excess scattering calculated with the fixed BR thickness of 4.5 nm in conjunction with eq. (3) (see, **II-2. Techniques**) may be overestimated. We therefore evaluated the excess scattering with the different BR thicknesses ranging from 4.5 nm to 16 nm (i.e., the maximum tail length of the BR, see **Figure 2C**). As summarized in the SI, we confirmed that the effects on the shapes of the excess scattering and the concentration profile are minimal (**Figures S4E** and **S4F**). We thus determined the mean values and uncertainties of the respective parameters ($\bar{L}$, $\boldsymbol{\varphi_m}$, σ_s, and z_1) in eq. (5).

III. 2. Structures of Bound Rubber – Molecular Dynamics Simulations

Figure 3A plots the volume fraction of BR chains as a function of z from the substrate surface calculated from the MD results. The mapping in terms of length unit (σ) was done by matching the average bond length of the simulated polymer chains to the approximate segment length of a PB monomer, l=0.965 σ.[68] From the figure we can see that the MD results with this length conversion of $1\sigma \approx 0.7$ nm are in good agreement with the SANS results (**Figure 3A**), indicating that the MD results reasonably predict the overall structure of the BR on the CB surface. We also extracted the distributions of trains, loops, and tails of the BR chains along the z-direction. As shown in **Figure 3B**, the peak at around 0.4σ ($\approx 0.3\ nm$) corresponds to the contributions of train segments, while the majority of the second peak at around 1.2σ ($\approx 0.8\ nm$) is the loop components. The tails are dominant at $z > 6\sigma$ ($\approx 4.2\ nm$), showing that they extend well into the matrix. The MD results also provide quantitative information about the tails, loops, and trains, as summarized in **Table 2**.

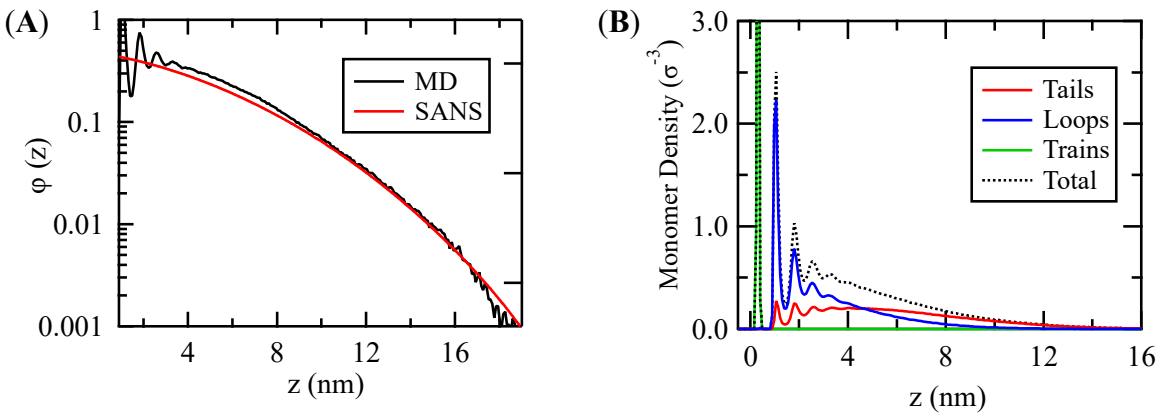

Figure 3. (**A**) Comparison of the polymer concentration profile of the BR layer for the loops and tail region between the SANS and MD results. Note that the beads (1σ in size, where $\sigma \approx$ 0.7 nm explains the SANS data well) form a monolayer after completely coating the substrate. The dip around 1σ is the boundary between the first coating and the next layer. (**B**) Monomer density distributions of trains, loops, and tails along the z-direction.

Table 2. Chain statistics of the simulated bound polymer chains[†]

Mole fraction			Effective grafting density (σ^{-2})	
tails	trains	loops	tails + loops	tails
0.35	0.20	0.45	0.274	0.004

[†]To estimate the effective grafting density of bound chains (considered as a Guiselin brush[34]), we counted the number of pseudo tails and loops by considering all tails and all loops having $n_{loop} > 1$ (note that $n_{oop} = 1$ are segments that belong to trains). The grafting density is, therefore, $\rho_T = (n_{tail} + 2n_{loop})/L_xL_y$, where L_xL_y is the area of a substrate and n_{tail} and n_{loop} are the number of tails and loops of a bound chain, respectively.

III. 3. Segmental Dynamics of Bound Rubber - Neutron Backscattering

Given the detailed structural information, we next focus on the dynamics of the BR chains. **Figure 4A** shows representative dynamic structure factor $S(q, E)$ for the BR-coated CB in dPB as well as (free) hPB chains blended in the dPB melt (hereafter assigned as "hPB in dPB") at $q = 4.7$ nm^{-1} and $T = 75$ °C. The total volume fraction of the free hPB in the dPB matrix was set equal to that for the BR-coated CB in dPB (3.1 vol %) such that the scattering contributions from H atoms are the same for both samples, allowing us to compare these two data sets directly. We first fit the $S(q,E)$ for the hPB in dPB sample with the Kohlrausch−Williams−Watts (KWW) equation,[69, 70] *i.e.*, an intermediate scattering function $S(q,t) \propto \exp[-(t/\tau_B(q))^{\gamma}]$ by applying the energy Fourier Transformation of $S(q, E)$ to fit in the energy domain, where $\tau_B(q)$ is the segmental relaxation time and γ is the stretching exponent. It has been reported that $\gamma \cong 0.5$ and power-law, $\tau_B{}^{\gamma}(q) \propto q^{-2}$ are established for many polymers in the limit of low q values ($q \leq 10$ nm^{-1}).[70] As shown in **Figure S6A**, the fits are in general good for the measured q-range with the fixed value of $\gamma = 0.5$. In addition, for $q < 10$ nm^{-1}, $\tau_B(q)$ shows the power-law behavior, $\tau_B{}^{0.5}(q) \propto q^{-2}$ (**Figure 4B**): we note that an exponent of $\gamma = 0.5$ for the segmental dynamics in polymer melts is predicted by the standard Rouse model[71] of polymer dynamics. At $q > 10$ nm^{-1}, a deviation from

the power-law become evident, indicating the non-Gaussian statistics of molecular displacements at the small length scales, as reported previously in the polymer melts including polyisoprene[72, 73], poly(ethylene oxide)[74], and PB.[75]

For the bound chains, at first glance, the spectra reasonably match those from the hPB in dPB sample except for small elastic contributions, as shown in **Figure 4A**. As shown in **Figure S2B**, the Guinier-type scattering from the internal voids of CB fillers that decreases with increasing q is evidenced, leading to one source of elastic contributions in $S(q, E)$. In addition, as Mark and co-workers indicated,[76] we expect additional elastic contributions originating from "immobile" segments strongly adsorbed on the CB surface. Note that CB has surface protons associated with functional groups such as COOH, but the quantity is negligible compared to protons in the BR layer of $\approx$ 9 nm in thickness. In order to further evaluate the spectra from the BR-coated CB in dPB, we approximate $S(q, E)$ as the sum of the KWW function and elastic contribution, *i.e.*,

$$S(q,E) = \left(A_{KWW}\mathfrak{F}\left[\exp\left[-\left(\frac{t}{\tau_B(q)}\right)^{\gamma}\right]\right] + A_d\delta(E)\right)\otimes R(q,E), \quad (8)$$

where A_{KWW} and A_{d} ($A_{\mathrm{KWW}}+A_{\mathrm{d}}=1$) are numerical constants and $\delta(E)$ is a delta function that is approximated to express an elastic contribution. $\mathfrak{F}$ denotes the Fourier transformation and $R(q,\mathrm{E})$ is the resolution function and $\otimes$ represents a convolution operator. Representative fitting results at 30°C are shown in **Figure S6B**, demonstrating that eq. (8) is appropriate regardless of q. The best-fits provide us the elastic contribution to be 0.48 ± 0.03 ($= A_d/(A_d + A_{KWW})$) at the q-range of 4.0 nm^{-1} $< q <$ 7.5 nm^{-1} at 30 °C, but it gradually decreases with increasing q, and finally saturates to a constant value of 0.20 ± 0.03 at q > 10 nm^{-1} (**Figure 4B**). As mentioned in the experimental section, deuterium also scatters incoherently (σ_{inc}= 2 barn), while H scatters with 80 barns. Taking the volume fraction of the BR (3.1%) into account, the total cross section from H amounts and D amounts in the BR-coated CB in dPB can be calculated to be 2.48 barn and 1.94 barn, respectively. We considered the ratio of the total cross section from H and D amounts for the calculation of the elastic contribution. As will be discussed later, the trains are immobile within the NBS time domain. The volume fraction of trains in the BR layer calculated from the MD results

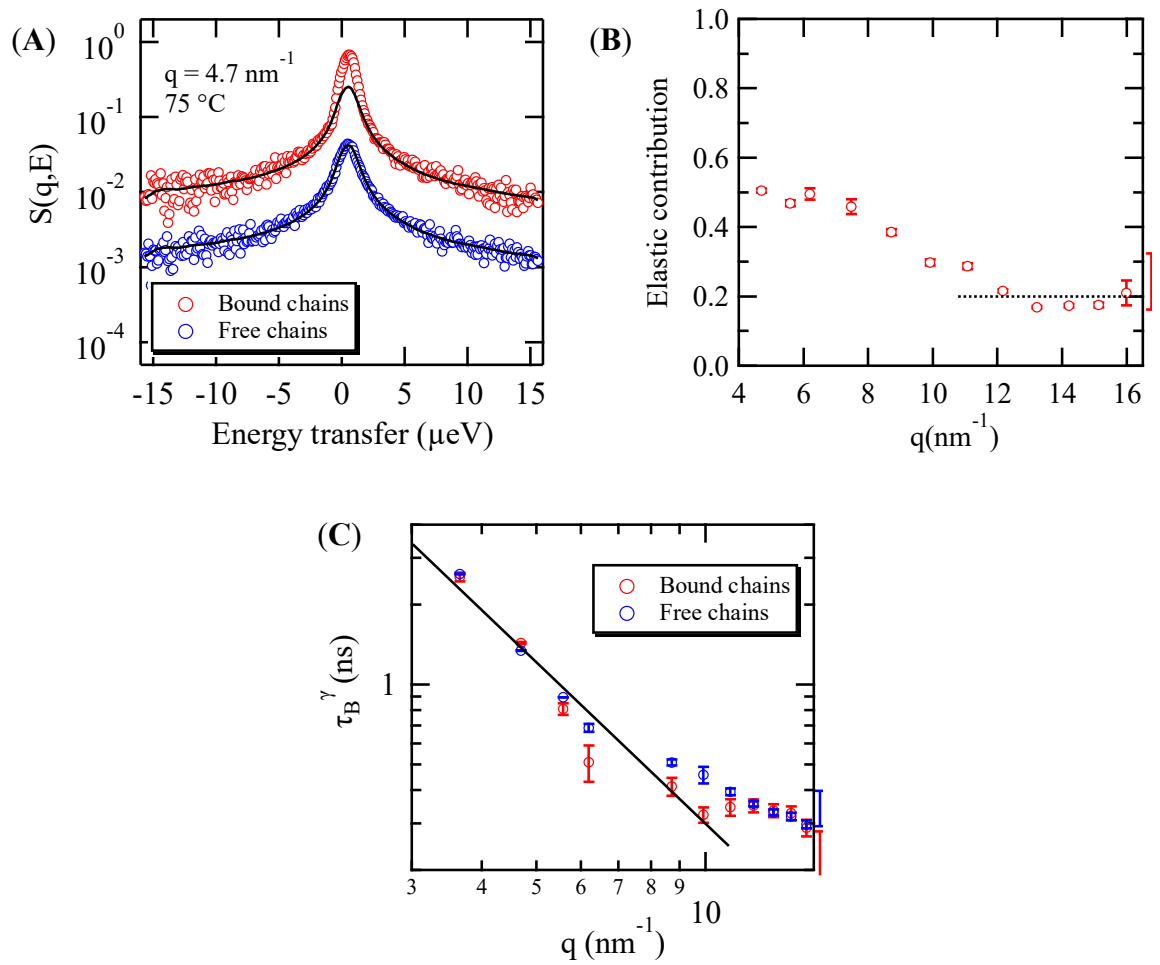

Figure 4. (**A**) Comparisons of NBS spectra for the hPB in dPB ("free chains") along with the BR-coated CB in dPB ("bound chains") at q = 4.7 nm^{-1} and 75 °C. The solid lines correspond to the best-fits of the KWW equation to the hPB in dPB sample. There are additional elastic contributions that result from residual scattering from the CB and immobile polymer (train) segments. The best-fits of eq. (8) to the data give us the overall elastic contributions (from the CB fillers and the BR chains), as summarized in (**B**) where the overall elastic contributions for the BR-coated CB in dPB are plotted as a function of q at 30 °C. The dotted line corresponds to the contributions from the immobile train components within the NBS time scale. (**C**) Local segmental relaxation times (τ_B) for the free and bound chains with the value of the stretch exponent (γ = 0.5) at 30 °C. For q < 10 nm^{-1}, the power-law behavior $\tau_B{}^{0.5} \sim q^{-2}$ (indicated in the solid line) holds.

is 0.2 (**Table 2**), which is in good agreement with the volume fraction of trains (*i.e.*, the inner layer) in the BR layer determined from the SANS results (**Figure 2C**). Hence, the elastic contribution of 0.20 ± 0.03 at $q > 10$ nm^{-1} seen in **Figure 4B** is attributed to the immobile trains within the NBS time domain. On the other hand, at $q < 10$ nm^{-1}, the additional elastic contribution from the CB fillers is identified in the NBS.

Figure 4C shows the q dependence of $\tau_B(q)$ for both the BR-coated CB in dPB and hPB in dPB. As they show nearly identical q-dependence, it is reasonable to conclude that the segmental motions remain unchanged between the bound chains and free chains in the melts. This result is consistent with the previous reports.[76-78] In the following section, we further aim at quantifying the contributions of the mobile and immobile components in conjunction with the MD results.

III. 4. Molecular Dynamics Simulations on Segmental Mean Square Displacements

In order to further understand the polymer-filler interface, we here focus on the MD simulation results. We calculated the mean square displacement (*MSD*) of the beads of bound chains as a function of the initial location from the filler surface (z) in the MD simulations (**Figure 5A**). The *MSD* is defined as

$$MSD = \langle [\vec{r_i}(t) - \vec{r_i}(0)]^2 \rangle \quad (9)$$

where $\vec{r_i}(t)$ is the location of the i^{th} bead after an elapsed time of t from its original location $\vec{r_i}(0)$. We hereafter assign polymer chains in a matrix as "unadsorbed chains". We considered all 2000 beads to calculate the MSD of the adsorbed and unadsorbed chains near the interface. We also assign the unadsorbed chains that locate far from the filler surface (i.e., $194\ \sigma < z < 204\ \sigma$ corresponding to the middle part of the simulation box (see **Table 1**) as "bulk" chains. For the bulk chains, we calculated the *MSD* by taking an average of the *MSD* curves of the middle 10% monomers of each chain (*i.e.*, 200 monomers) to minimize the effect of chain ends. The crossover behavior for the bulk from the Rouse regime ($MSD \sim t^{1/2}$) to the reptation regime ($MSD \sim t^{1/4}$)[79] is observed at the crossover time (τ_e) indicated by the arrows in **Figure 5A, 5B, and 5D**, $\tau_e \approx 5{,}500\tau$.

In order to identify the z dependence of the *MSDs* of both adsorbed and unadsorbed chains, we calculated the *MSD* of monomers as a function of the distance (z) from the filler surface. Based

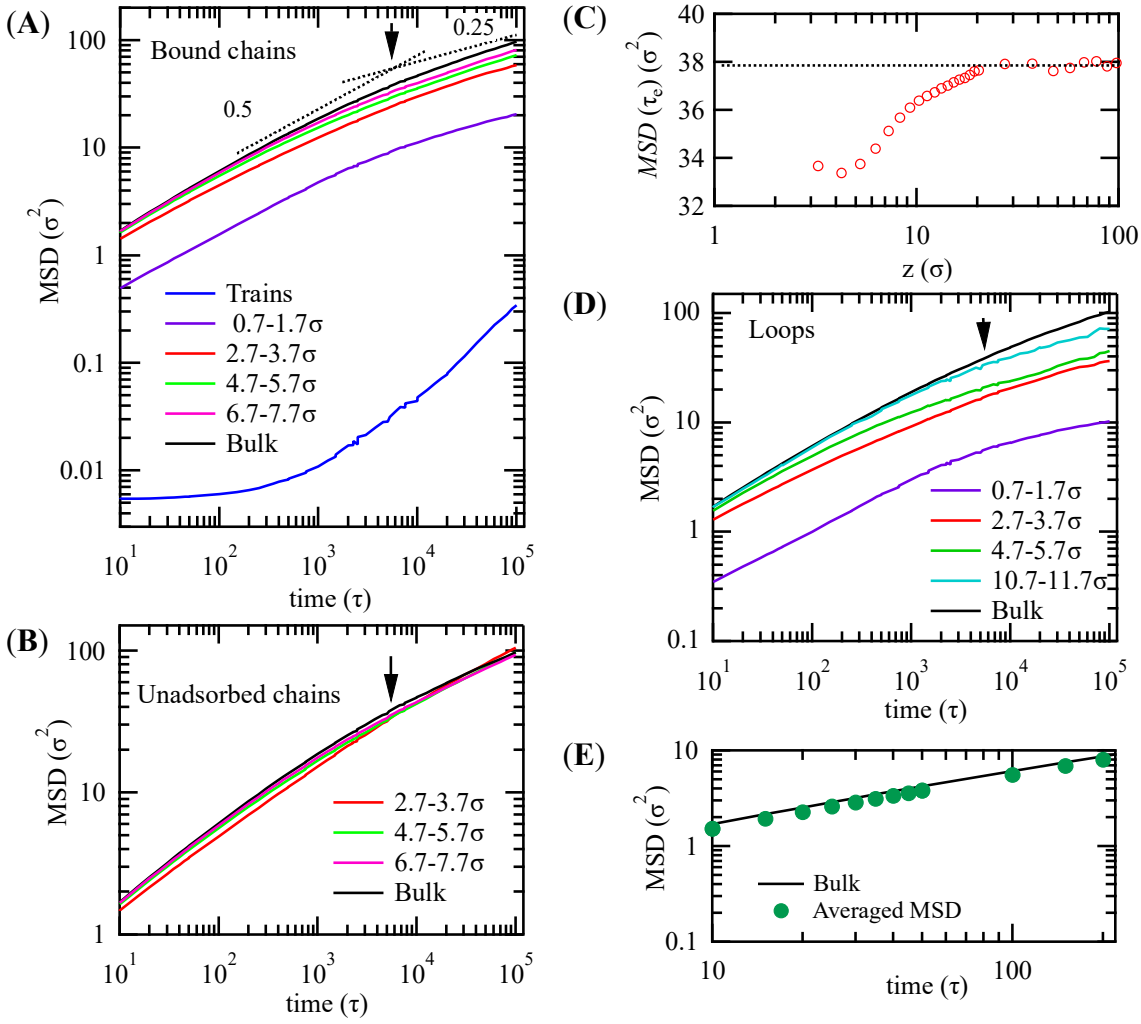

Figure 5. Calculated *MSD* of (**A**) the BR chains, (**B**) unadsorbed chains near the filler surface at the given distances from the filler surface. For comparison, the *MSD* of middle monomers of the unadsorbed chain (bulk) is also plotted. The arrows correspond to $\tau_e \approx 5{,}500\tau$ for the bulk. (**C**) *MSD* values at the bulk cross-over time, $MSD(\tau_e)$, are plotted as a function of z. The dotted line corresponds to the bulk $MSD(\tau_e)_{\text{bulk}} \approx 37.85\sigma^2$. (**D**) Calculated *MSD* of the loops estimated by eq. (10) at the given distances from the filler surface. (**E**) *MSD* of the bound chains in the vicinity of the filler surface (like in (**A**)) but extended to show the behavior at the relevant NBS time scale. The symbols (indicated in green) correspond to an average *MSD* of the mobile (loop/tails) components. See the main text for the details.

on the monomer density profiles shown in **Figure 3B**, we found that the region at $0 < z < 0.7\sigma$ is composed of only trains, while the loops and tails coexist at above $z > 0.7\ \sigma$. As shown in **Figure**

5A, the *MSD* of trains is considerably suppressed compared to the bulk, while the *MSD* of the bound chains at $z > 0.7\ \sigma$ (*i.e.*, a mixture of loops and tails) increases with increasing z and becomes nearly equivalent to that of the bulk chains. Remarkably, the deviations from the $MSD \sim t^{1/2}$ power-law takes place at around $2.7\ \sigma < z < 3.7\sigma$, where the loops are a majority component. We note, in pure polymer melts, these deviations relate to the transition from Rouse motion ($t^{1/2}$) to local reptation ($t^{1/4}$) that occurs at $t \cong \tau_e$, while for loops it reflects their finite size. In this context, the 30 % to 50 % smaller *MSD* within the MD time window at around $2.7\ \sigma < z < 3.7\sigma$ is rationalized. In addition, the segmental dynamics of unadsorbed chains near the filler surface are slightly slowed down within the Rouse regime due to the presence of loops and tails, but they escape the "obstacles" and recover the bulk-like reptation dynamics at sufficiently long times (**Figure 5B**). To further illuminate these, we calculated the *MSD* at the bulk cross-over time ($\tau_e \approx 5{,}500\tau$), $MSD(\tau_e)$, for the unadsorbed chains as a function of z. As shown in **Figure 5C,** the $MSD(\tau_e)$ values for the unadsorbed chains located within the bound layer (up to $z < 20\ \sigma$, see **Figure 3A and 3B**) are lower than the bulk value ($MSD(\tau_e)_{bulk} = 37.85\sigma^2$), but increases with increasing z, and approaches to the bulk value at $z > 20\ \sigma$. Hence, a decrease in the segmental dynamics of the unadsorbed chains due to the obstacles is indicative.

To further extract the *MSD* of loops (MSD_{loop}) alone, we approximated the observed *MSD* (MSD_{total}) at $z > 0.7\ \sigma$ as a linear combination of MSD_{loop} and *MSD* of tails (MSD_{tail}):

$$MSD_{total} = \eta MSD_{loop} + (1 - \eta) MSD_{tail} \quad (10)$$

where η is the fraction of loops in the bound chains at the given distances determined from the monomer density profiles (**Figure 3B)** and we assume that MSD_{tail} is equal to the bulk *MSD*. Based on the monomer density profiles shown in **Figure 3B**, we could estimate the fraction of loops in the bound chains at the different z values (**Table S1)**.

Figure 5D shows MSD_{loop} estimated by using eq. (10) at the four different regimes near the filler surface. Overall, the chain dynamics of loops is suppressed due to the topological constrains, but the magnitude of the *MSD* is significantly higher than that of trains within the overall simulation time window. Specially, the MSD_{loop} at $10.7\ \sigma < z < 11.7\sigma$ exhibits the bulk

behavior at $t < \tau_e$, while a deviation from the bulk behavior is indicated at $t > \tau_e$ since loops fixed at their anchor points do not have a transiently existing virtual tube. The results also indicate that the time when the deviation from the $MSD \sim t^{1/2}$ power-law occurs for loops are of similar magnitude to the bulk (or tails). However, we should stress that the chain conformations of tails and loops are quite different: the tails are more stretched than the loops (**Figure 3B**). This trend is consistent with previous experimental results on loops and their linear counterparts (brushes or tails) on planar solid substrates[80] and with a previous prediction using a polymer density fluctuation theory.[81] We postulate that the structural dissimilarities of tails and loops lead to a marked difference in their interdigitation with neighboring unadsorbed chains. Shull used the numerical self-consistent field treatment and showed that loops have less interdigitation with neighboring free chains compared to their linear (tail) counterparts.[82] However, this argument may be dependent on the size of loops. Richter and co-workers used well-characterized polymer rings (by analogy for loops[83]) in linear polymer matrices and concluded that larger loops are interdigitated, while small loops do not allow the interdigitation of linear chains.[84] The same group separately reported that the loops of physiosorbed (unentangle) polymer chains on nanopore surfaces interdigitate with matrix polymer chains, resulting in the entanglement-like dynamics.[12] Hence, we anticipate that the presence of large loops formed on the CB filler allows the interdigitation of matrix polymer chains, while the tails do entangle with the matrix polymer. In this way, the filler-polymer interface can establish a strong connectivity between a matrix and filler via the BR/interphase, which will be further described in the following section of the neutron spin echo results. Detailed MD results on the dynamics of trains, loops, and tails with different degree-of-polymerization N values will be summarized in a forthcoming paper.

We can now compare the results from the MD simulations with the NBS results. From the comparison of the computational ($\tau_e \approx 5{,}500\tau$) and experimental τ_e values (**Figure S7D**) for the hPB in dPB sample, the conversion factors for the respective temperatures were set. As shown in **Figure 5A**, we can see that the calculated MSD values for the train components are nearly constant ($\approx 6.0 \times 10^{-3}\sigma^2$, which is equivalent to $2.9 \times 10^{-3}\, nm^2$) within the corresponding

NBS time window (*i.e.*, t < 180 τ at 150 ℃, the highest temperature used for the NBS measurements). Hence, the motion amplitude, *i.e.*, $S(q,t)/S(q,0)\sim\exp[-q^2(MSD)/6]$, for the train components is close to 1. This indicates that the q-independent plateau at q > 12 nm^{-1} shown in **Figure 4B** cannot be related to any intrinsic length scale but is due to the immobile fraction of the trains.

Moreover, as shown in **Figure 5A**, the *MSD* of the mobile tail and loop components at $0.7\,\sigma < z < 1.7\sigma$ within the relevant NBS time window is about three times smaller than the bulk, while that at $1.7\,\sigma < z < 2.7\sigma$ almost recovers the bulk behavior. This suggests a local heterogeneity in the segmental dynamics within such a very small space (~ a 1 nm-distance from the filler surface) due to chain binding, as predicted previously.[36, 37] Hence, it is reasonable to conclude that the quasielastic scattering we measured using NBS corresponds to the sum of the *MSDs* of the tail and loop components at $0.7\,\sigma < z < 1.7\sigma$ and the *MSDs* at z >1.7σ (which can be approximated as the MSD of the bulk) by their compositions. Considering that the fraction of loops and tails located at $0.7\,\sigma < z < 1.7\sigma$ is estimated to be 16 % relative to the overall loop and tail components (**Figure 3B**), we found that the average *MSD* of the loops and tails is nearly identical to the bulk as shown in **Figure 5E** (represented as symbols), supporting the NBS results shown in **Figure 4C**.

III. 5. Dynamics at the Chain Level - Neutron Spin Echo

Given the direct evidence on the local segmental dynamics of the BR chains, we next focus on the dynamics at the chain level measured by NSE. **Figure 6A** shows a representative normalized intermediate dynamic structure factor, $S(q,t)/S(q,0)$, for the BR-coated CB in dPB at q =2 nm^{-1} and 100 °C. For comparison, $S(q,t)/S(q,0)$ for the hPB in dPB sample is also plotted. It has been well documented that NSE is an ideal tool to study the entropy-driven Rouse dynamics on an intermediate length scale and the local reptation motions (*i.e.*, laterally confined chain dynamics) on a larger length scale in the melt[70]. Following the established protocols, we first characterized the Rouse rate, $Wl^4 = 3k_BTl^2/\zeta$ ($k_B$is the Boltzmann constant, T is the absolute temperature, and

ζ is the monomer friction coefficient), and the tube diameter (d_t) for the hPB in dPB sample. The details are summarized in **Figure S7**. In addition, as summarized in **Figure 6D**, the temperature dependence of the tube diameter is evidenced, as reported previously,[52] while the magnitude is larger than the reported value (3.6 nm) that was based on rheology results.[52]

For the BR-coated CB in dPB sample, the single chain dynamics of the BR chains are significantly slowed down compared to that of the hPB in dPB sample within the NSE time window (**Figure 6A**). As mention above, there are the elastic contributions of CB fillers within the q range used for NSE. Hence, we first calculated $S(q,t)/S(q,0)_{BR}$ for the BR using the following relation which accounts for the immobile contributions of the CB fillers estimated from the SANS results:

$$\frac{S(q,t)}{S(q,0)_{total}} = (1-c)\frac{S(q,t)}{S(q,0)_{BR}} + c \times \frac{S(q,t)}{S(q,0)_{CB}}, \quad (11)$$

where $S(q,t)/S(q,0)_{total}$ and $S(q,t)/S(q,0)_{CB}$ are the observed normalized intermediate dynamic structure factor and the normalized intermediate dynamic structure factor for the CB filler ($S(q,t)/S(q,0)_{CB}$=1), respectively, and c is the elastic contribution from CB fillers that depends on q (see, **Figure S8A** for the detailed procedure). **Figure 6B** shows representative $S(q,t)/S(q,0)_{BR}$ at the four different q values and 100 °C (the fitting results at the other temperatures are summarized in **Figure S8B to D**). For unentangled polydimethylsiloxane (PDMS) in anodic aluminum oxide (AAO) where q-dependent plateauing of $S(q,t)$ was observed, Richter and coworkers reported a suppression of long wavelength Rouse modes when an unentangled polymer chain adsorb on a solid surface.[12] Motivated by their results, we fit the NSE data with their model at $t < \tau_e$, where $\tau_e = d_t^4/(\pi^2 W l^4)$. The dotted line (indicated in red) in **Figure 6A** shows the best-fit of the suppressed Rouse mode to the data, suggesting that the initial slowdown in $S(q,t)/S(q,0)_{BR}$ can be well explained by the presence of mode restrictions with multiple anchoring points. As mentioned for the hPB in dPB sample, the deviation from the Rouse mode is ascribed to the local reptation. However, in contrast to PDMS in AAO, we find q-independent plateaus at long times that cannot

be related to an intrinsic length scale like the tube diameter. The result must relate to an immobile fraction of the train segments, as discussed above.

We further analyze the NSE data for the bound chains. Schneider and co-workers studied the segmental dynamics of polymer chains bound to silica filler surfaces in unentangled poly(ethylene glycol) and poly (butylene oxide) marices using a contrast-matched NSE technique. Based on a two-phase model assuming that bound polymer chains are composed of immobile and mobile (bulk-like) parts, they quantified the amount of the immobile part and the segmental dynamics of the mobile part.[78] Here we apply the same two-phase model to the present NSE data. At spatial and time windows beyond the Rouse regime, long chains are confined by their mutual entanglements,[79] leading to a retardation of the decay of a structure factor. In the reptation model, this lateral confinement is captured by the tube diameter. Hence, the following equation was adopted to analyze the tube diameter of the BR chains:

$$\frac{S(q,t)}{S(q,0)_{BR}} = \mu + (1-\mu) \times \left(\left[1 - \exp\left(-\frac{Qq^2 d_t^2}{36} \right) \right] S_{local}(q,t) + \exp\left(-\frac{q^2 d_t^2}{36} \right) S_{esc}(q,t) \right) \quad (12)$$

where μ is the fraction of immobile polymer components, and $S_{local}(q,t)$ and $S_{esc}(q,t)$ are the contributions from local Rouse motion along the tube and escape from the tube, respectively.[70] The present polymer architecture (*i.e.*, bound chains) does not allow the chain to escape as the one end is stuck to the filler surface. Also, in the NSE time window, the chains do not escape from the tube ($t \ll$ the longest Rouse relaxation time $\tau_R \cong$ 2600 ns at 150 °C). Hence, we set $S_{esc}(q,t) = 1$. The local reptation part is expressed as $S_{local}(q,t) = \exp\left[(t/\tau_0) erfc(\sqrt{(t/\tau_0)}) \right]$, where $\tau_0 = 36/(Wl^4q^4)$ is the time scale for the Rouse motion along the tube. The Rouse rates (Wl^4) for the BR-coated hPB in dPB were fixed to those of the free chains, as clarified above. The fitting ranges were set to $t > \tau_e$ and we confirmed that the accessible time window covers at least twice τ_e. **Figure 6B** and **Figure S8B to D** show the best-fits of eq. (12) to the NSE data at the four different q values, giving us an elastic fraction of $\mu \approx 0.3$ regardless of temperature (**Figure 6C**). This value suggests that not only the trains ($\approx$ 20 % in the BR chains) but also the very short loops located at $0.7\,\sigma < z < 1.7\sigma$ (see, **Figure 5A**, the corresponding volume fraction in the bound chain

is estimated to be about 14 % based on the monomer density profiles shown in **Figure 3B**) are immobile within the NSE time and space domains. On the other hand, as discussed above, the other loop components and tails are mobile and interactive with matrix polymer chains, resulting in a strong rubber-filler "interlocking" interphase which play vital roles in rubber reinforcement including low loss modulus (*i.e.*, low rolling resistance) of filler reinforced elastomers.[85]

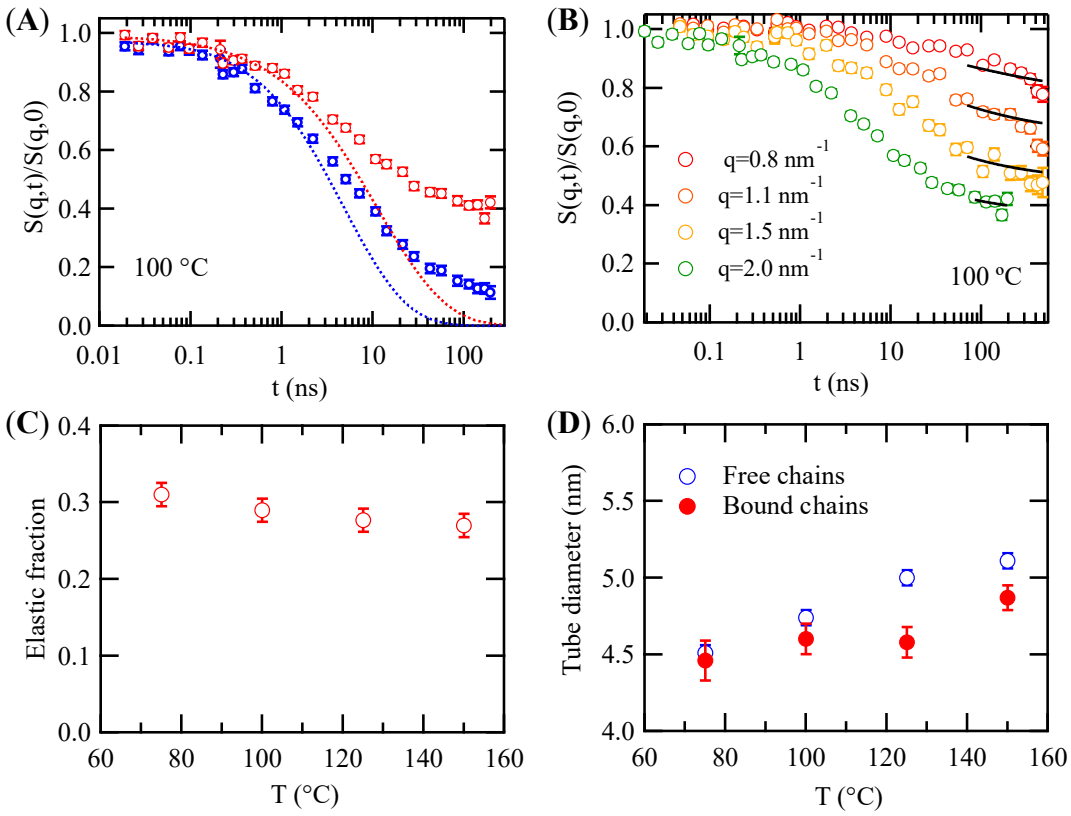

Figure 6. (**A**) Comparison of $S(q,t)/S(q,0)$ between the bound (indicated in red) and free (indicated in blue) chains at 100 ºC and q = 2.0 nm^{-1} is shown. It should be noted that $S(q,t)/S(q,0)$ for the bound chain is corrected for the immobile contributions of the CB fillers using eq. (11). The red dotted line corresponds to the best-fit of the suppressed Rouse dynamics[12] for the BR-coated CB in dPB, while the blue dotted line corresponds to the best-fit of the unrestricted Rouse mode.[70] The number of suppressed Rouse modes was set to 6, while the distribution of the mode number used in Ref. 12 was not considered for the fit. (**B**) $S(q,t)/S(q,0)_{BR}$ for the BR-coated CB in dPB at the given four q values and 100 ºC. The solid lines correspond to the best-fits of eq. (12) to the data. Temperature dependences of the elastic fraction (**C**) and tube diameter of the BR chains obtained from the best-fits of eq. (12) to the data (**D**) are shown. The tube diameter of free chains measured by using the hPB in dPB sample is also plotted (**D**).

Figure 6D summarizes the temperature dependence of the tube diameter of the bound chains. It should be noted that since there is no tube for loops, the tube diameter obtained from the fitting of eq. (12) gives us a "confinement length" that limits the monomer motions by the size. The results indicate that the temperature dependence of the confinement length is much weaker than that of the bulk. Therefore, the present results can be explained as follows: Since the tails are reaching far out from the filler surface into the bulk, they adapt the tube diameter of the bulk. On the other hand, the loops fixed at their anchor points don't change in size with temperature. Hence, the confinement length is composed of the two contributions: (i) the tube size of the tail (bulk, d_{bulk}) that increases with temperature (as shown in **Figure 6D**) and (ii) the confinement length of loops (d_{loop}) that is more or less fixed regardless of temperature. To first order, one may add these effects, but further experimental and simulations studies are required to derive the exact correlation between these effects. NSE experiments using grafted brushes (by analogy for tails) or polymer rings (by analogy for loops) in a polymer melt will help us separate the contributions of loops and tails in a quantitative manner. At the same time, detailed MD analysis will allow us to calculate the dynamic structure factors for loops and tails separately.

While a previous report showed that the tube diameter of the matrix polymer remained unchanged when the filler loading is below the percolation threshold,[86] the present result is the direct evidence of the chain entanglements of the bound chains. Using short (unentangled) chemically grafted chains, Mark and co-workers also reported that the topological confinement within a "cone" spanned by neighboring grafted chains (the grafting density of $\approx$ 0.6 nm^{-2}) leads to a narrower tube diameter.[76] Hence, the present NSE data indicates that the effect of tail-tail interactions is minimal for physisorbed chains. This is further confirmed by the MD results that give us the "effective" grafting density of tails to be 0.004 σ^{-2} (or ~ 0.006 nm^{-2}) (**Table 2**).

IV. Conclusions

We have studied the structures and dynamics of the BR layer formed on the CB filler surfaces in the melt (below the percolation threshold) by combining neutron techniques and MD

simulations. The combined results reveal the novel structural and dynamical features of the BR chains for the emergence of rubber reinforcement: (i) the structural partition of the BR chains into three components (*i.e.*, trains, loops, and tails) with their fractions; (ii) their dynamical hierarchies, *i.e.*, the trains that remain immobile on the filler surface, the loops that are fairly large and hence allow the interdigitation of matrix chains, and the tails with their unique characteristics to reach far out into the matrix and entangle with matrix chains.

As demonstrated in **Figure S2**, the mechanical enhancement associated with using the BR is well-known for several decades in the rubber industry, but the mechanism behind this reinforcement remains unexplained. Given the structures and dynamics of the BR, we are now able to discuss the correlation with the macroscopic mechanical enhancement. Our results indicate the existence of entanglements/interdigitation of the BR chains with neighboring polymer chains in a matrix, leading to a well-developed and adhesive interphase. In addition, the chain entanglement/interdigitation at the interphase region causes an additional interfacial friction, reducing the flow of a matrix polymer and thus enhancing the elastic property. At the same time, we anticipate that the trains, which may correspond to the so-called "glassy layer" reported in polymer nanocomposites[11, 87, 88], act as strong anchoring points during deformation[88]. As a consequence, when CB-filled elastomers are deformed, the above two characteristics of the BR chains and interphase permit external stresses to be transferred effectively from a weak, deformable polymer matrix to a strong, rigid CB filler. Further experiments and simulations for high filler loading reinforced rubbers above the percolation threshold deserve future work.

According to the Energy Technology Perspectives 2017,[89] in 2050 the total number of cars globally will be three times greater than that in 2010, signifying a pressing demand for new materials. Thus, the development of advanced reinforced synthetic rubbers with balanced, superior performance including durability and safety is critical to meet this demand due to the dwindling availability of natural resources. However, the optimization of filler-enforced elastomers is complicated and multi-faceted problem. For example, wet grip is determined by the relaxation behavior at high frequencies, while rolling resistance is related to the dissipation at low

frequencies.[33] In addition, from an industrial point of view, the origins of reinforcement (such as impact fracture, wear performance, wet grip performance, fuel efficiency, fatigue fracture) are diverse depending on the structures and dynamics of a polymer at different length scales (angstrom-scale to micron-scale) and temporal scales (1 fs to s). Hence, the development of advanced filler reinforced synthetic rubbers relies on the interconnected knowledge of polymer and fillers' hierarchical structures and dynamics utilizing integrated measurements and analysis. This would then allow us to establish a comprehensive structure-dynamics-property relationship for filler-reinforced rubbers.

Author Information

Corresponding Authors

Email: tadanori.koga@stonybrook.edu (T. K.)

Email: michihiro.nagao@nist.gov (M. N.)

Author Contributions

T. K. and M. N. conceptualized and designed the study. T. K., D. S., M. N., M. T., and B. F. performed the neutron scattering and spectroscopy experiments. J. M. Y. C. and B. G. S. performed the MD simulations. T. M. and H. K. prepared the samples. T. M., H. K., and B. M. Y. performed the rheology experiments. A. R. performed the TEM experiments. T. K., D. S., J. M. Y. C., T. T., M. T., M. K., B. F., D. R., M. N. participated in the data analysis. T. K. wrote the manuscript with editing input from all the other authors. All authors have given approval to the final version of the manuscript.

Notes

The authors declare no competing financial interest. The identification of any commercial product or trade name does not imply endorsement or recommendation by NIST.

Acknowledgements

Acknowledgment is made to the Donors of the American Chemical Society Petroleum Research Fund for partial support of this research (T.K.). Access to the NGB30m-SANS, HFBS, and CHRNS-NSE was provided by the Center for High Resolution Neutron Scattering, a partnership between the National Institute of Standards and Technology and the National Science Foundation under Agreement No. DMR-2010792. The computational/simulations aspect of this work were performed at the Center for Nanophase Materials Sciences, a U.S. Department of Energy Office of Science User Facility. This research also used resources of the Oak Ridge Leadership Computing Facility, which is a DOE Office of Science User Facility supported under Contract DE-AC05-00OR22725. The synchrotron radiation experiments were performed at the BL20XU of SPring-8 with the approval of the Japan Synchrotron Radiation Research Institute (JASRI) (Proposal No. 2017A1374).

Supporting Information Available.

Figure S1. Determination of the percolation threshold for CB/PB PNCs and filler size distribution

Figure S2. Stress-strain curve for CB filled PB.

Figure S3. Degradation check for the BR-coated CB in dPB.

Figure S4. SANS/USAXS data for the BR-coated CB in dPB, SANS data for the CB in dPB and hPB/dPB blend samples.

Figure S5. Discussion about a different polymer density model to fit the SANS data.

Figure S6. Additional NBS results.

Figure S7. NSE results for the hPB in dPB sample.

Figure S8. $S(q,t)/S(q,0)$ for the BR-coated CB in dPB sample.

Table S1. Volume fraction of loops calculated by the MD simulations.

Discussion about the effect of sample preparation.

This material is available free of charge *via* the Internet at http://pubs.acs.org.

References

1. Kumar, S. K. , Benicewicz, B. C. , Vaia, R. A. and Winey, K. I. 50th Anniversary Perspective: Are Polymer Nanocomposites Practical for Applications? *Macromolecules* **2017**, 50, 714-731.

2. Bailey, E. J. and Winey, K. I. Dynamics of polymer segments, polymer chains, andnanoparticles in polymer nanocomposite melts: A review. *Prog. Polym. Sci.* **2020**, 105, 101242.

3. Koenig, J. L. The Chemical Reactions of Network Structures in Elastomers. *Acc. Chem. Res.* **1999**, 32, 1-8.

4. Jancar, J. , Douglas, J. F. , Starr, F. W. , Kumar, S. K. , Cassagnau, P. , Lesser, A. J. , Sternstein, S. S. and Buehler, M. J. Current Issues in Research on Structure-Property Relationships in Polymer Nanocomposites. *Polymer* **2010**, 51, 3321−3343.

5. Schneider, G. J. Dynamics of nanocomposites. *Curr. Opin. Chem. Eng.* **2017**, 16, 65-77.

6. Twiss, D. F. The theory of vulcanisation. *J. Soc. Chem. Ind.* **1925**, 44, 106-108.

7. Bansal, A. , Yang, H. , Li, C. , Cho, K. , Benicewicz, B. C. , Kumar, S. K. and Schadler, L. S. Quantitative equivalence between polymer nanocomposites and thin polymer films. *Nat. Mater.* **2005**, 4, 693-698.

8. Ciprari, D. , Jacob, K. and Tannenbaum, R. Characterization of polymer nanocomposite interphase and its impact on mechanical properties. *Macromolecules* **2006**, 39, 6565-6573.

9. Pastorino, C. , Binder, K. , Kreer, T. and Müller, M. Static and dynamic properties of the interface between a polymer brush and a melt of identical chains. *J. Chem. Phys.* **2006**, 124, 064902.

10. Oh, H. and Green, P. F. Polymer chain dynamics and glass transition in athermal polymer/nanoparticle mixtures. *Nat. Mater.* **2009**, 8, 139-143.

11. Papon, A. , Montes, H. , Hanafi, M. , Lequeux, F. , Guy, L. and Saalwächter, K. Glass-Transition Temperature Gradient in Nanocomposites: Evidence from Nuclear Magnetic Resonance and Differential Scanning Calorimetry. *Phys. Rev. Lett.* **2012**, 108, 065702.

12. Krutyeva, M. , Wischnewski, A. , Monkenbusch, M. , Willner, L. , Maiz, J. , Mijangos, C. , Arbe, A. , Colmenero, J. , Radulescu, A. , Holderer, O. , Ohl, M. and Richter, D. Effect of Nanoconfinement on Polymer Dynamics: Surface Layers and Interphases. *Phys. Rev. Lett.* **2013**, 110.

13. Medalia, A. I. Morphology of aggregates 6. Effective volume of aggregates of carbon black from electron microscopy. Application to vehicle absorption and to die swell of filled rubber. *J. Colloid Interface Sci.* **1970**, 32, 115-131.

14. Dannenberg, E. M. Bound rubber and carbon black reinforcement. *Rubber Chem. Technol.* **1986**, 59, 512-524.

15. Kenny, J. C. , McBrietry, V. J. , Rigbi, Z. and Douglass, D. C. Carbon black filled natural rubber 1. Structural investigations. *Macromolecules* **1991**, 24, 436-443.

16. Yurekli, K. , Krishnamoorti, R. , Tse, M. F. , McElrath, K. O. , Tsou, A. H. and Wang, H. C. Structure and dynamics of carbon black-filled elastomers. *J. Polym. Sci., Part B: Polym. Phys.* **2001**, 39, 256-275.

17. Berriot, J. , Lequeux, F. , Monnerie, L. , Montes, H. , Long, D. and Sotta, P. Filler-elastomer interaction in model filled rubbers, a H-1 NMR study. *J. Non-Cryst. Solids* **2002**, 307, 719-724.

18. Papon, A. , Guy, T. C. L. , Saalwachter, K. , Oberdisse, J. , Merabia, S. , Long, D. , Sotta, P. , Frielinghaus, H. H. , Radulescu, A. , Deme, B. , Noirez, L. , Montes, H. and Lequeux, F. Studying model samples to understand mechanical Properties of filled Elastomers. *KgK Kautsch. Gummi Kunst.* **2013**, 66, 52−58.

19. Harton, S. E. , Kumar, S. K. , Yang, H. C. , Koga, T. , Hicks, K. , Lee, E. , Mijovic, J. , Liu, M. , Vallery, R. S. and Gidley, D. W. Immobilized Polymer Layers on Spherical Nanoparticles. *Macromolecules* **2010**, 43, 3415-3421.

20. Jouault, N. , Moll, J. F. , Meng, D. , Windsor, K. , Ramcharan, S. , Kearney, C. and Kumar, S. K. Bound Polymer Layer in Nanocomposites. *ACS Macro Lett.* **2013**, 2, 371-374.

21. Jiang, N. , Endoh, M. K. , Koga, T. , Masui, T. , Kishimoto, H. , Nagao, M. , Satija, S. K. and Taniguchi, T. Nanostructures and Dynamics of Macromolecules Bound to Attractive Filler Surfaces. *ACS Macro Lett.* **2015**, 4, 838-842.

22. Baeza, G. P. , Dessi, C. , Costanzo, S. , Zhao, D. , Gong, S. , Alegria, A. , Colby, R. H. , Rubinstein, M. , Vlassopoulos, D. and Kumar, S. K. Network dynamics in nanofilled polymers. *Nat. Commun.* **2016**, 7, 11368.

23. Griffin, P. J. , Bocharova, V. , Middleton, L. R. , Composto, R. J. , Clarke, N. , Schweizer, K. S. and Winey, K. I. Influence of the Bound Polymer Layer on Nanoparticle Diffusion in Polymer Melts. *ACS Macro Lett.* **2016**, 5, 1141-1145.

24. Jouault, N. , Crawford, M. K. , Chi, C. , Smalley, R. J. , Wood, B. , Jestin, J. , Melnichenko, Y. B. , He, L. , Guise, W. E. and Kumar, S. K. Polymer Chain Behavior in Polymer Nanocomposites with Attractive Interactions. *ACS Macro Lett.* **2016**, 5, 523−527.

25. Koga, T. , Barkley, D. , Nagao, M. , Taniguchi, T. , Carrillo, J.-M. Y. , Sumpter, B. G. , Masui, T. , Kishimoto, H. , Koga, M. , Rudick, J. G. and Endoh, M. K. Interphase structures and dynamics near nanofiller surfaces in polymer solutions. *Macromolecules* **2018**, 51, 9462-9470.

26. Jimenez, A. M. , Zhao, D. , Misquitta, K. , Jestin, J. and Kumar, S. K. Exchange Lifetimes of the Bound Polymer Layer on Silica Nanoparticles. *ACS Macro Lett.* **2019**, 8, 166-171.

27. Popov, I. , Carroll, B. , Bocharova, V. , Genix, A.-C. , Cheng, S. , Khamzin, A. , Kisliuk, A. and Sokolov, A. P. Strong Reduction in Amplitude of the Interfacial Segmental Dynamics in Polymer Nanocomposites. *Macromolecules* **2020**, 53, 4126-4135.

28. Chen, Q. , Gong, S. , Moll, J. , Zhao, D. , Kumar, S. K. and Colby, R. H. Mechanical Reinforcement of Polymer Nanocomposites from Percolation of a Nanoparticle Network. *ACS Macro Lett.* **2015**, 4, 398-402.

29. Merabia, S. , Sotta, P. and Long, D. R. A microscopic model for the reinforcement and the nonlinear behavior of fllled elastomers and themoplastic elastomers (Payne and Mullins effects). *Macromolecules* **2008**, 41, 8252-8266.

30. Zhao, D. , Ge, S. , Senses, E. , Akcora, P. , Jestin, J. and Kumar, S. K. Role of Filler Shape and Connectivity on the Viscoelastic Behavior in Polymer Nanocomposites. *Macromolecules* **2015**, 48, 5433-5438.

31. Zhou, Y. , Yavitt, B. M. , Zhou, Z. , Bocharova, V. , Salatto, D. , Endoh, M. K. , Ribbe, A. E. , Sokolov, A. P. , Koga, T. and Schweizer, K. S. Bridging Controlled Network Microstructure and Long Wavelength Fluctuations in Silica-Poly(2-vinylpyridine) Nanocomposites: Experimental Results and Theoretical Analysis *Macromolecules* **2020**, 53, 6984-6994.

32. Yavitt, B. M. , Salatto, D. , Zhou, Y. , Huang, Z. , Endoh, M. , Wiegart, L. , Bocharova, V. , Ribbe, A. E. , Sokolov, A. P. , Schweizer, K. S. and Koga, T. Collective Nanoparticle Dynamics Associated with Bridging Network Formation in Model Polymer Nanocomposites. *ACS Nano* **2021**, 15, 11501-11513.

33. Mujtaba, A. , Keller, M. , Ilisch, S. , Radusch, H.-J. , Thurn-Albrecht, T. , Saalwachter, K. and Beiner, M. Mechanical properties and cross-link density of styrene-butadiene model composites containing fillers with bimodal particle size distribution. *Macromolecules* **2012**, 45, 6504-6515.

34. Mujtaba, A. , Keller, M. , Ilisch, S. , Radusch, H. J. , Beiner, M. , Thurn-Albrecht, T. and Saalwachter, K. Detection of Surface-Immobilized Components and Their Role in Viscoelastic Reinforcement of Rubber-Silica Nanocomposites. *ACS Macro Lett.* **2014**, 3, 481-485.

35. Karatrantos, A. , Composto, R. J. , Winey, K. I. , Kröger, M. and Clarke, N. Modeling of Entangled Polymer Diffusion in Melts and Nanocomposites: A Review. *Polymers* **2019**, 11, 876/1-29.

36. Starr, F. W. , Schrøder, T. B. and Glotzer, S. C. Molecular Dynamics Simulation of a Polymer Melt with a Nanoscopic Particle. *Macromolecules* **2002**, 35, 4481-4492.

37. Starr, F. W. , Douglas, J. F. , Meng, D. and Kumar, S. K. Bound Layers “Cloak” Nanoparticles in Strongly Interacting Polymer Nanocomposites. *ACS Nano* **2016**, 10, 10960-10965.

38. Scheutjens, J. M. H. M. and Fleer, G. J. Statistical theory of the adsorption of interacting chain molecules. 2. Train, loop, and tail size distribution. *J. Phys. Chem.* **1980**, 84, 178-190.

39. Simha, R. , Frisch, H. L. and Eirich, F. R. The Adsorption of Flexible Macromolecules. *The J. Phys. Chem.* **1953**, 57, 584-589.

40. Guiselin, O. Irreversible Adsorption of a Concentrated Polymer-Solution. *Europhys Lett.* **1992**, 17, 225-230.

41. Marzolin, C. , Auroy, P. , Deruelle, M. , Folkers, J. P. , Leger, L. and Menelle, A. Neutron Reflectometry Study of the Segment-Density Profiles in End-Grafted and Irreversibly Adsorbed Layers of Polymer in Good Solvents. *Macromolecules* **2001**, 34, 8694-8700.

42. Cotton, J. P. , Nierlich, M. , Boue, F. , Daoud, M. , Farnoux, B. , Jannink, G. , Duplessix, R. and Picot, C. Experimental determination of the temperature–concentration diagram of flexible polymer solutions by neutron scattering *J. Chem. Phys.* **1976**, 65, 1101.

43. de Gennes, P. G. Dynamique d'une couche de polymères adsorbés. *C. R. Acad. Sci. Paris Ser. II* **1986**, 302, 765-768.

44. Koga, T. , Hashimoto, T. , Takenaka, M. , Aizawa, K. , Amino, N. , Nakamura, M. , Yamaguchi, D. and Koizumi, S. New insight into hierarchical structures of carbon black dispersed in polymer matrices: A combined small-angle scattering study. *Macromolecules* **2008**, 41, 453-464.

45. Eggers, H. and Schummer, P. Reinforcement Mechanisms in Carbon Black and Silica Loaded Rubber Melts at Low Stresses. *Rubber Chem. Technol.* **1996**, 69, 253-265.

46. Shibayama, M. , Matsunaga, T. and Nagao, M. Evaluation of incoherent scattering intensity by tranmission and sample thickness. *J. Appl. Cryst.* **2009**, 42, 621-628.

47. Beaucage, G. Approximatiions Leading to a Unified Exponetial/Power -Law Approach to Small-Angle Scattering. *J. Appl. Cryst.* **1995**, 28, 717-728.

48. Azuah, R. T. , Kneller, L. R. , Qiu, Y. M. , Tregenna-Piggott, P. L. W. , Brown, C. M. , Copley, J. R. D. and Dimeo, R. M. DAVE: A Comprehensive Software Suite for the Reduction,

Visualization, and Analysis of Low Energy Neutron Spectroscopic Data. *J. Res. Natl. Inst. Stand. Technol.* **2009**, 114, 341-358.

49. Meyer, A. , Dimeo, R. M. , Gehring, P. M. and Neumann, D. A. The high-flux backscattering spectrometer at the NIST Center for neutron reserach. *Rev. Sci. Instrum.* **2003**, 74, 2759-2777.

50. Arbe, A. , Richter, D. , Colmenero, J. and Farago, B. Merging of the a and b relaxations in polybutadiene: A neutron spin echo and dielectric study. *Phys. Rev. E* **1996**, 54, 3853-3869.

51. Carrillo, J. M. Y. , Cheng, S. W. , Kumar, R. , Goswami, M. , Sokolov, A. P. and Sumpter, B. G. Untangling the Effects of Chain Rigidity on the Structure and Dynamics of Strongly Adsorbed Polymer Melts. *Macromolecules* **2015**, 48, 4207-4219.

52. Fetters, L. J. , Lohse, D. J. , Richter, D. , Witten, T. A. and Zirkel, A. Connection between Polymer Molecular Weight, Density, Chain Dimensions, and Melt Viscoelastic Properties. *Macromolecules* **1994**, 27, 4639-4647.

53. Khodabakhshi, S. , Fulvio, P. F. and Andreoli, E. Carbon black reborn: Structure and chemistry for renewable energy harnessing. *Carbon* **2020**, 162, 604-649.

54. Wang, M.-J. , Wolff, S. and Donnet, J.-B. Filler-Elastomer Interactions. Part III. Carbon-Black-Surface Energies and Interactions with Elastomer Analogs. *Rubber Chem. Technol.* **1991**, 64, 714-736.

55. Richter, D. and Kruteva, M. Polymer dynamics under confinement *Soft Matter* **2019**, 15, 7316-7349

56. Suzuki, N. , Yatsuyanagi, F. , Ito, M. and Kaidou, H. Effects of surface chemistry of silica particles on secondary structure and tensile properties of silica-filled rubber systems. *J. Appl. Polym. Sci.* **2002**, 86, 1622-1629.

57. Kremer, K. and Grest, G. S. Dynamics of Entangled Linear Polymer Melts - a Molecular-Dynamics Simulation. *J. Chem. Phys.* **1990**, 92, 5057-5086.

58. Rieker, T. P. , Hindermann-Bischoff, M. and Ehrburger-Dolle‡, F. Small-Angle X-ray Scattering Study of the Morphology of Carbon Black Mass Fractal Aggregates in Polymeric Composites. *Langmuir* **2000**, 16, 5588-5592.

59. Speck, J. S. , Endo, M. and Dresselhaus, M. S. Structure and intercalation of thin benzene derived carbon fibers. *J. Cryst. Growth* **1989**, 94, 834-848.

60. Takenaka, M. , Nishitsuji, S. , Amino, N. , Ishikawa, Y. , Yamaguchi, D. and Koizumi, S. Structure Analyses of Swollen Rubber-Filler Systems by Using Contrast Variation SANS. *Macromolecules* **2009**, 42, 308-311.

61. Papon, A. , Montes, H. , Hanafi, M. , Lequeux, F. , Guy, L. and Saalwachter, K. Glass-Transition Temperature Gradient in Nanocomposites: Evidence from Nuclear Magnetic Resonance and Differential Scanning Calorimetry. *Phys. Rev. Lett.* **2012**, 108, 065702.

62. Mortazavian, H. , Fennell, C. J. and Blum, F. D. Structure of the Interfacial Region in Adsorbed Poly(vinyl acetate) on Silica. *Macromolecules* **2016**, 49, 298-307.

63. Borodin, O. , Smith, G. D. , Bandyopadhyaya, R. and Byutner, E. Molecular dynamics study of the influence of solid interfaces on poly(ethylene oxide) structure and dynamics. *Macromolecules* **2003**, 36, 7873-7883.

64. Barbier, D. , Brown, D. , Grillet, A. C. and Neyertz, S. Interface between end-functionalized PEO oligomers and a silica nanoparticle studied by molecular dynamics simulations. *Macromolecules* **2004**, 37, 4695-4710.

65. Kritikos, G. and Terzis, A. F. Variable density self consistent field study on bounded polymer layer around, spherical nanoparticles. *Eur. Polym. J.* **2013**, 49, 613-629.

66. Zajac, R. and Chakrabarti, A. Irreversible polymer adsorption from semidilute and moderately dense solutions. *Phys. Rev. E* **1995**, 52, 6536-6549.

67. Karim, A. , Satija, S. K. , Douglas, J. F. , Ankner, J. F. and Fetters, L. J. Neutron reflectivity study of the density profile of a model end-grafted polymer brush: influencne of solvent quality. *Phy. Rev. Lett.* **1994**, 73, 3407.

68. Carrillo, J. M. Y. and Sumpter, B. G. Structure and dynamics of confined flexible and unentangled polymer melts in highly adsorbing cylindrical pores *J. Chem. Phys.* **2014**, 141, 074904.

69. Richter, D. , Monkenbusch, M. , Arbe, A. and Colmenero, J. Neutron scattering and the glass transition in polymers – present status and future opportunities. *J. Non-Cryst. Solids* **2001**, 287, 286−296.

70. Richter, D. , Monkenbusch, M. , Arbe, A. and Colmenero, J. Neutron Spin Echo in Polymer Systems. *Adv. Polym. Sci.* **2005**, 174, 1-221.

71. Arbe, A. , Colmenero, J. , Monkenbusch, M. and Richter, D. Dynamics of Glass-Forming Polymers: "Homogeneous" versus "Heterogeneous" Scenario. *Phys. Rev. Lett.* **1998**, 81, 590−593.

72. Arbe, A. , Colmenero, J. , Alvarez, F. , Monkenbusch, M. , Richter, D. , Farago, B. and Frick, B. Non-Gaussian Nature of the α Relaxation of Glass-Forming Polyisoprene. *Phys. Rev. Lett.* **2002**, 89, 245701.

73. Arbe, A. , Colmenero, J. , Alvarez, F. , Monkenbusch, M. , Richter, D. , Farago, B. and Frick, B. Experimental evidence by neutron scattering of a crossover from Gaussian to non-Gaussian behavior in the α relaxation of polyisoprene. *Phys. Rev. E* **2003**, 67, 051802.

74. Krutyeva, M. , Martin, J. , Arbe, A. , Colmenero, J. , Mijangos, C. , Schneider, G. J. , Unruh, T. , Su, Y. and Richter, D. Neutron scattering study of the dynamics of a polymer melt under nanoscopic confinement *J. Chem. Phys.* **2009**, 131, 174901.

75. Roh, J. H. , Tyagi, M. , Hogan, T. E. and Roland, C. M. Space-Dependent Dynamics in 1,4-Polybutadiene Nanocomposite. *Macromolecules* **2013**, 46, 6667-6669.

76. Mark, C. , Holderer, O. , Allgaier, J. , Hübner, E. , Pyckhout-Hintzen, W. , Zamponi, M. , Radulescu, A. , Feoktystov, A. , Monkenbusch, M. , Jalarvo, N. and Richter, D. Polymer Chain Conformation and Dynamical Confinement in a Model One-Component Nanocomposite. *Phys. Rev. Lett.* **2017**, 119, 047801.

77. Yang, J. , Melton, M. , Sun, R. , Yang, W. and Cheng, S. Decoupling the Polymer Dynamics and the Nanoparticle Network Dynamics of Polymer Nanocomposites through Dielectric Spectroscopy and Rheology. *Macromolecules* **2020**, 53, 302-311.

78. Glomann, T. , Hamm, A. , Allgaier, J. , Hübner, E. G. , Radulescu, A. , Farago, B. and Schneider, G. J. A microscopic view on the large scale chain dynamics in nanocomposites with attractive interactions. *Soft Matter* **2013**, 9, 10559-10571.

79. Doi, M. and Edwards, S. F., *The Theory of Polymer Dynamics*. Clarendon Press: Oxford, 1986.

80. Patton, D. , Knoll, W. and Advincula, R. C. Polymer Loops vs. Brushes on Surfaces: Adsorption, Kinetics, and Viscoelastic Behavior of α,ω-Thiol Telechelics on Gold. *Macromol. Chem. Phys.* **2011**, 212, 485-497.

81. Cao, D. and Wu, J. Surface Forces between Telechelic Brushes Revisited: The Origin of a Weak Attraction. *Langmuir* **2006**, 22, 2712-2718.

82. Shull, K. Theory of end-adsorbed polymer brushes in polymeric matrices *J. Chem. Phys.* **1991**, 94, 5723.

83. Divandari, M. , Morgese, G. , Trachsel, L. , Romio, M. , Dehghani, E. S. , Rosenboom, J.-G. , Paradisi, C. , Zenobi-Wong, M. , Ramakrishna, S. N. and Benetti, E. M. Topology Effects on the Structural and Physicochemical Properties of Polymer Brushes. *Macromolecules* **2017**, 50, 7760-7769.

84. Kruteva, M. , Allgaier, J. and Richter, D. Direct Observation of Two Distinct Diffusive Modes for Polymer Rings in Linear Polymer Matrices by Pulsed Field Gradient (PFG) NMR. *Macromolecules* **2017**, 50, 9482-9493.

85. Le, H. H. , Reincke, K. , Das, A. , Stöckelhuber, K.-W. , Wiessner, S. , Pham, T. , Do, Q. K. , Hoang, X. T. , Grellmann, W. , Heinrich, G. and Radusch, H.-J. Filler Wetting in Miscible ESBR/SSBR Blends and Its Effect on Mechanical Properties. *Macromol. Mater. Eng.* **2016**, 301, 414−422.

86. Schneider, G. J. , Nusser, K. , Willner, L. , Falus, P. and Richter, D. Dynamics of Entangled Chains in Polymer Nanocomposites. *Macromolecules* **2011**, 44, 5857-5860.

87. Berriot, J. , Montes, H. , Lequeux, F. , Long, D. and Sotta, P. Evidence for the Shift of the Glass Transition near the Particles in Silica-Filled Elastomers. *Macromolecules* **2002**, 35, 9756-9762.

88. Jouault, N. , Dalmas, F. , Said, S. , Cola, E. D. , Schweins, R. , Jestin, J. and Boué, F. Direct small-angle-neutron-scattering observation of stretched chain conformation in nanocomposites: More insight on polymer contributions in mechanical reinforcement. *Phys. Rev. E* **2010**, 82, 031801.

89. https://www.iea.org/etp/publications/etp2017/.